PROGRESS IN AEROSPACE AND AVIATION TECHNOLOGY
e-ISSN: 2821-2924

PAAT

Vol. 5 No. 1 (2025) 55-84
https://publisher.uthm.edu.my/ojs/index.php/paat

Aerodynamic Study of a Single Groove on The Upper and Lower Surfaces of an Airfoil at Low Angles of Attack

Muhammad Aideed Azman[1], Mohd Fauzi Yaakub[1]*, Esmail Abdullah[1], Wan Muhammad Aqil Wan Nawang[1]

[1] *Research Center for Unmanned Vehicle (RECUV), Faculty of Mechanical and Manufacturing Engineering, Universiti Tun Hussein Onn Malaysia, 86400 Parit Raja, Johor, MALAYSIA*

*Corresponding Author: fauziy@uthm.edu.my
DOI: https://doi.org/10.30880/paat.2025.05.01.006

Article Info

Received: 27 February 2025
Accepted: 11 June 2025
Available online: 30 June 2025

Keywords

Angle of attack, lift coefficient, drag coefficient, simulation, aerodynamics, groove, airfoil

Abstract

This project investigates the aerodynamic effects of introducing a single groove on both the upper and lower surfaces of a NACA 0012 airfoil at low angles of attack, ranging from 0° to 10°. Each simulation features two grooves, one on the upper surface and one on the lower surface, to evaluate their combined influence on lift and drag performance. The objective is to determine whether passive flow control via surface grooves can enhance aerodynamic efficiency in low-speed conditions. The study was conducted using computational fluid dynamics (CFD) simulations in ANSYS Fluent. Several groove configurations were analyzed, including parallel grooves at 0.20C, 0.25C, and 0.30C, as well as fixed upper grooves at 0.25C and 0.30C combined with variable lower groove positions at 0.25C to 0.40C. A mesh independence test and validation against experimental data were performed to ensure simulation accuracy. A groove diameter of 1.0 cm was selected based on its favorable aerodynamic performance across the tested angles of attack. Results indicate that the configuration with a fixed upper groove at 0.25C and a lower groove at 0.40C yields the most significant lift improvement and slight drag reduction compared to the baseline airfoil. The study demonstrates that using two grooves in a dual-surface configuration can effectively delay flow separation and enhance the lift-to-drag ratio. These findings support the advancement of passive aerodynamic control strategies in low-speed airfoil applications.

1. Introduction

Airfoils play a key role in aerodynamics for uses like aircraft wings, rotor blades, propellers, and wind turbines. Their ability to create lift and limit drag affects the efficiency, stability, and control of these systems. At low angles of attack, airflow usually stays close to the surface, leading to a steady lift. However, flow separation can occur in some cases, which reduces performance and increases drag.

Passive flow control methods, which include changing the shape of the airfoil surface, have become popular for improving performance in low-Reynolds-number flows without needing extra energy. One method is adding grooves to the surface. These grooves can strengthen the boundary layer and delay or lessen flow separation, which may improve the lift-to-drag ratio. How well grooves work depends on their depth, width, and position along the chord. When used on a symmetric airfoil like the NACA 0012, they offer useful ideas for better low-speed aerodynamics.

Research on airfoil aerodynamics, particularly surface modifications for flow control, has advanced considerably. Kundu et al. [1] outlined fundamental fluid mechanics principles applied to aerodynamics,

This is an open access article under the CC BY-NC-SA 4.0 license.

emphasizing boundary layer dynamics and airfoil shape influences on lift and drag. Suprayitno et al. [2] explored airfoil optimization under uncertain conditions, showing that minor geometric adjustments can enhance performance metrics like lift coefficients in variable flows.

Studies on grooved airfoils highlight potential benefits. Ismail et al. [3] analyzed the NACA 4415 airfoil, revealing angle-of-attack impacts on lift, drag, and pitching moments, with surface features affecting pressure distribution. Kilavuz et al. [4] examined flow around torpedo-like geometries, finding attack angles influence separation patterns, extendable to airfoil grooves altering local flows. Klose et al. [5] conducted direct numerical simulations on cambered airfoils at Reynolds number 20,000, identifying surface indentations inducing vortices that energize boundary layers and delay stall.

Additional contributions include ElJack and Soria [6], who detailed the cycle of laminar separation bubbles over the NACA 0012 airfoil, noting surface perturbations reforming bubbles to reduce drag. Akbar et al. [7] experimentally validated NACA 0012 performance, underscoring grooves' role in modulating pressure gradients. These studies correlate positively, indicating grooves enhance lift-to-drag ratios by promoting attached flow, especially at low speeds.

However, contradictions and ambiguities exist. While Suprayitno et al. [2] and Klose et al. [5] found that grooves consistently improve lift, Ismail et al. [3] noticed that at steeper angles, they can increase drag, indicating that the benefits depend on the design. Ambiguities arise in optimal groove placement; ElJack and Soria [6] advocate leading-edge positioning for bubble reformation, whereas Kilavuz et al. [4] indicate mid-chord benefits for pressure recovery. There are still unanswered questions about how dual-surface grooves work on symmetric airfoils at low angles (0°–10°), uneven shapes, and their impact in slow, incompressible flows, since most previous studies have mainly looked at single-surface grooves or high-Reynolds-number situations.

This study evaluates the aerodynamic effects of a single groove on both upper and lower surfaces of the NACA 0012 airfoil at low angles of attack (0°–10°), optimizing lift and drag through varied groove sizes, shapes, and positions. By addressing correlations (e.g., groove-induced boundary layer energization), contradictions (e.g., lift gains versus drag increases), ambiguities (e.g., ideal placement), and gaps (e.g., dual-surface effects in low-speed regimes), it provides a framework for passive flow control in applications like unmanned aerial vehicles and wind turbines.

The approach employs computational fluid dynamics simulations via ANSYS Fluent, using a 1.0 m chord airfoil under steady, incompressible, 2D conditions at 43.9 m/s free-stream velocity. Groove configurations—parallel, fixed upper with varying lower positions, and diameters (0.5 cm, 1.0 cm, 1.5 cm)—are tested to quantify lift coefficient (Cl), drag coefficient (Cd), and pressure distributions. Validation against experimental benchmarks (e.g., from Ashby and Fowlkes [8]) and grid independence tests ensure reliability. This methodology resolves ambiguities via asymmetrical placement comparisons, bridges gaps through dual-groove analyses, and contextualizes results for discussions on velocity contours, vortex formation, and practical recommendations, identifying optimal designs (e.g., upper groove at 0.25C with lower at 0.40C) for enhanced low-speed performance.

2. Methodology

The methodology employed in this study follows a systematic approach, as illustrated in the flowchart of Fig. 1. This process is divided into three key phases: pre-research preparations, computational fluid dynamics (CFD) simulations using ANSYS Fluent, and result interpretation. Initially, geometric and operating parameters—such as the NACA 0012 airfoil profile, chord length, angles of attack (0° to 10° in 2° increments), groove configurations (parallel and asymmetrical placements), and free-stream velocity (43.9 m/s)—are defined. SolidWorks is utilized to model the baseline airfoil and incorporate groove modifications, exporting files in IGS format. Subsequently, ANSYS Fluent facilitates the simulation workflow, encompassing geometry import and rotation for angle-of-attack variations, domain construction, meshing with refined inflation layers for boundary layer resolution, setup of material properties and boundary conditions, and solution execution with monitoring of lift and drag coefficients. Finally, the results are checked against experimental data, confirmed for grid independence, and the aerodynamic factors are studied using coefficients and flow visuals to see how the grooves affect the baseline. This structured framework ensures reliable assessment of passive flow control strategies in low-speed aerodynamics.

Progress in Aerospace and Aviation Technology Vol. 5 No. 1 (2025) p. 55-84

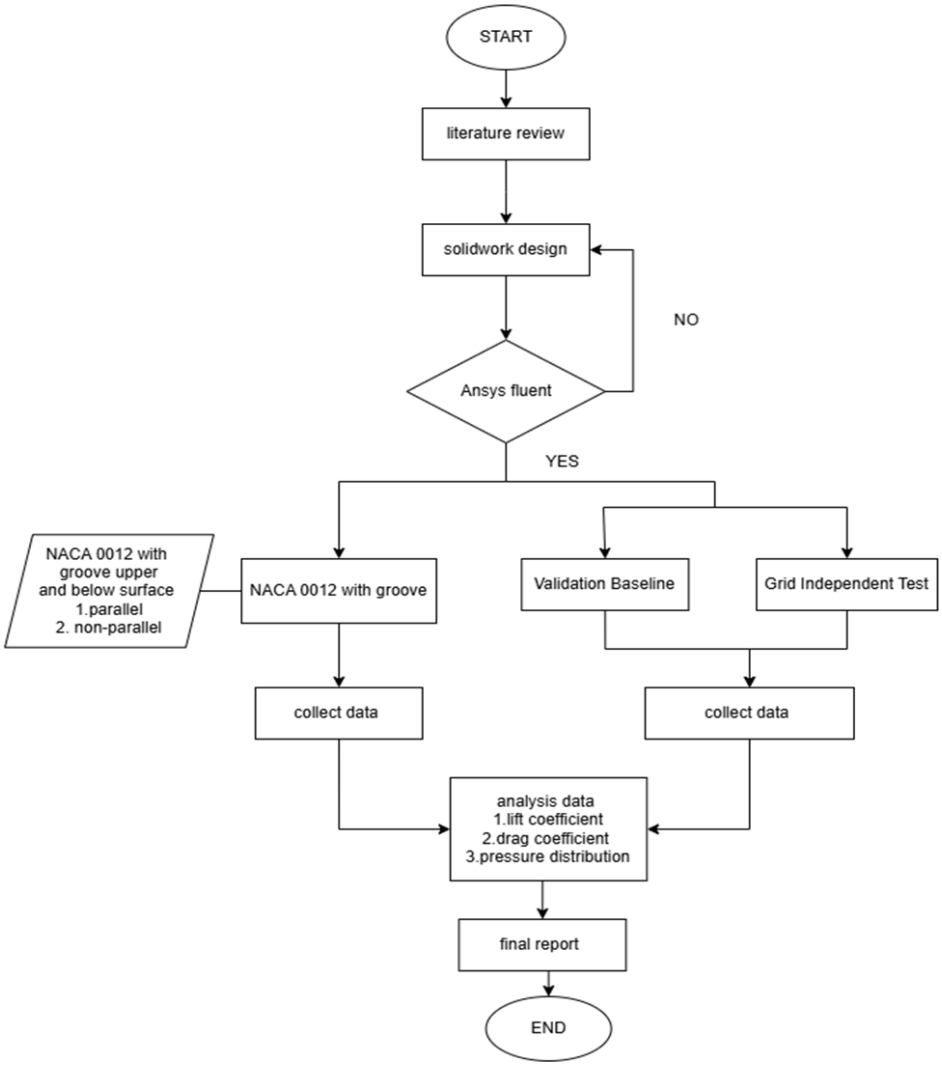

Fig. 1 *Research flowchart*

2.1 Geometric and Operating Setup

This study uses the symmetrical NACA 0012 airfoil to investigate the effects of surface grooves on aerodynamic performance. Simulations were conducted with a 1.0 m chord length and groove placements at positions like 0.25C and 0.30C. The angle of attack ranged from 0° to 10° in 2° steps under steady, incompressible, 2D flow conditions at 43.9 m/s, representing low-speed aerodynamic environments. The summary of the airfoil geometry and operating condition is given in Table 1.

Table 1 *Summary of airfoil geometry and operating condition*

Parameter	Description
Airfoil Type	NACA 0012
Chord Length	1.0 meter
Angle of Attack (AoA)	0°, 2°, 4°, 6°, 8°, 10°
Groove Shape	Circular Arc (Concave indentation)
Flow Regime	Steady, incompressible, 2D planar
Free-stream Velocity	43.9 m/s
Reynolds Number Range	10^5 to 10^6
Mach Number	≈ 0 (incompressible assumption)
Test Objective	to evaluate lift and drag at low angles of attack

2.2 Grid Independent Test (GIT)

Grid Independent Test (GIT) refers to a critical validation procedure in computational fluid dynamics (CFD) simulations, designed to confirm that the numerical results are independent of the mesh resolution and thus reliable for further analysis. In the context of this study, the GIT evaluates the sensitivity of aerodynamic parameters—specifically the lift coefficient (Cl) and drag coefficient (Cd)—to variations in mesh density across different angles of attack (AoA) for the NACA 0012 airfoil. In this study, three different mesh densities were generated for the airfoil geometry within a C-type computational domain, as detailed in Table 2. Multiple mesh configurations, characterized by node counts ranging from 60,450 to 136,730, were tested under steady, incompressible, 2D flow conditions at a free-stream velocity of 43.9 m/s. The process involves running simulations for each mesh at AoA values from 0° to 10° in 2° increments and comparing the resulting Cl and Cd values. The test demonstrates that differences in outcomes across this node range are minimal, indicating convergence and stability in the simulation results. This ensures that the selected mesh (with sufficient resolution, including 15 inflation layers for boundary layer capture) accurately resolves flow features such as separation and vortices without undue computational expense, thereby enhancing the credibility of the CFD analysis for groove-modified airfoils.

Table 2 Mesh *configuration and description*

Number of nodes	Type of mesh	Description
136730	Fine mesh	High refinement with dense boundary layer meshing using inflation layers
92390	Medium mesh	Moderately refined mesh, particularly around the airfoil surface
60450	Coarse Mesh	Larger elements with fewer layers near the boundary

2.3 Difference Groove Size

Table 3 shows the three different groove sizes that were tested to identify the most suitable diameter that offers aerodynamic improvement without introducing excessive drag. The grooves were implemented on the upper surface of the NACA 0012 airfoil at a fixed position of 0.25C from the leading edge, as shown in Fig. 2.

Table 3 *Groove size variants and their chordwise ratios*

Groove diameter (cm)	Chordwise ratio (d/C)	Placement position	Shape of groove
0.5 diameter	0.005	0.25 C	Circular arc
1.0 diameter	0.010	0.25 C	Circular arc
1.5 diameter	0.015	0.25 C	Circular arc

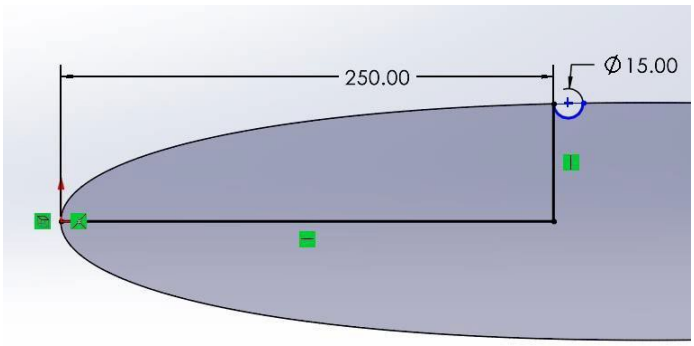

Fig. 2 *Groove positioned at 0.25C on the upper surface of the NACA 0012 airfoil with a 15 mm circular arc indentation*

2.4 Groove Design Configuration

In this study, several groove configurations were introduced on the NACA 0015 airfoil, focusing on different orientations and positions. The designs include parallel grooves aligned with the flow direction and fixed grooves positioned at specific chordwise locations on the upper surface. In all configurations, the grooves are circular with a diameter of 1 cm, and only two grooves are activated in each simulation, one on the upper surface and one on the lower surface.

Progress in Aerospace and Aviation Technology Vol. 5 No. 1 (2025) p. 55-84

2.4.1 Parallel Groove

This configuration involves the placement of grooves in a parallel arrangement along the chord line on both the upper and lower surfaces of the NACA 0015 airfoil. Fig. 3 shows the geometry of NACA0015 with parallel grooves. The grooves are positioned symmetrically at specific chordwise locations to examine their influence on boundary layer development and overall aerodynamic performance. Three groove positions were tested in this study: (i) parallel groove at 0.20c, (ii) parallel groove at 0.25c and (iii) parallel groove at 0.30c.

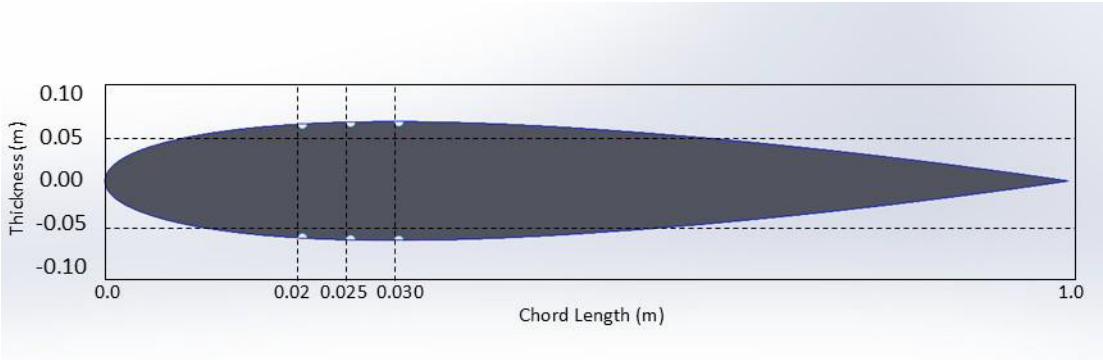

Fig. 3 *Geometry of NACA 0015 with parallel grooves located at 0.20C, 0.25C, and 0.30C on both upper and lower surfaces*

2.4.2 Fixed Upper Groove at 0.25C with Varying Lower Groove Positions

In this configuration, a single groove is fixed at 25% of the chord length (0.25C) from the leading edge on the upper surface of the NACA 0015 airfoil. Fig. 4 shows the location of the fixed single upper groove at 0.25C. This position is selected due to its proximity to the leading edge, where the boundary layer is still in its early laminar stage. Introducing a disturbance at this location can help energize the boundary layer, reduce the risk of early flow separation, and potentially enhance lift generation. While the upper surface groove remains fixed at 0.25C for all test cases, the lower surface groove is varied across multiple positions to evaluate the effect of asymmetrical groove placement. Specifically, the groove on the lower surface is placed at 0.25C, 0.30C, 0.35C, and 0.40C, respectively, in separate simulations.

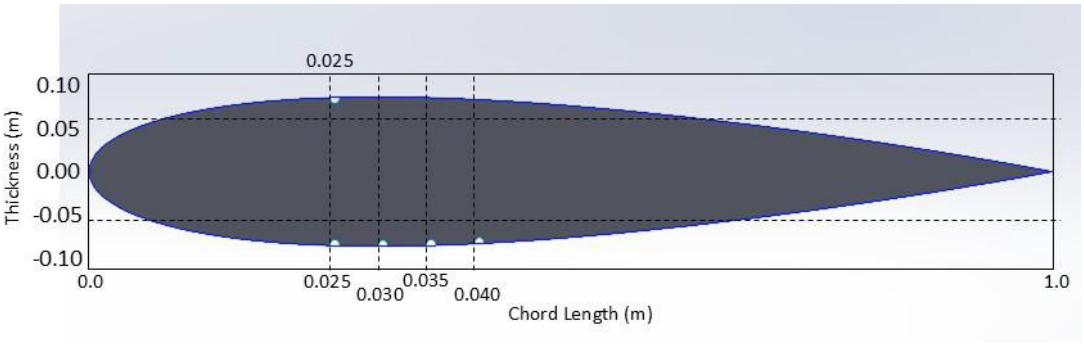

Fig. 4 *Fixed upper groove at 0.25C with varying lower groove positions at 0.25C, 0.30C, 0.35C, and 0.40C*

2.4.3 Fixed Upper Groove at 0.30C with Varying Lower Groove Positions

In this configuration, a single groove is fixed at 30% of the chord length (0.30C) from the leading edge on the upper surface of the airfoil. Fig. 5 shows the location of the fixed single upper groove at 0.30C. This location is selected to target the region where the boundary layer begins to transition from laminar to turbulent flow. Applying a disturbance at this position is intended to help sustain attached flow and delay separation, contributing to improved aerodynamic efficiency. To assess the effects of asymmetrical groove placement, the groove on the lower surface is varied across three different positions in separate simulations: 0.30C, 0.35C, and 0.40C. While the groove on the upper surface remains constant at 0.30C, these variations on the lower surface enable a comparative analysis of how downstream surface disturbances influence flow behaviour and lift-to-drag characteristics.

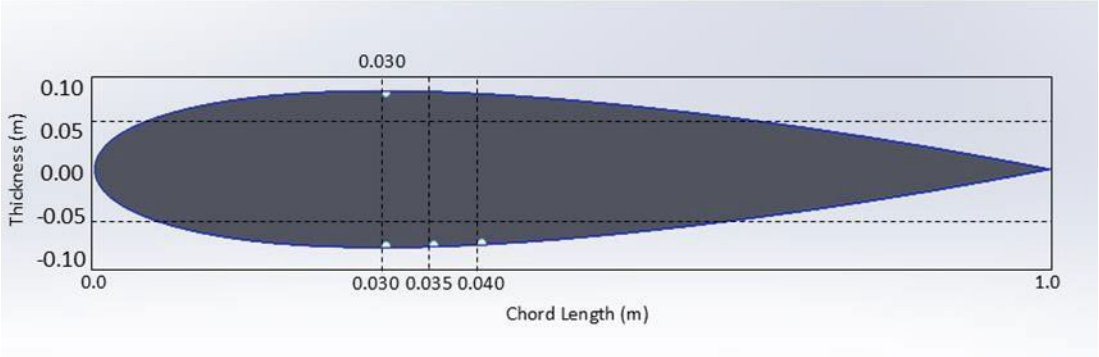

Fig. 5 *Fixed upper groove at 0.30C with varying lower groove positions at 0.30C, 0.35C, and 0.40C*

2.5 Tools and Software

This project involved using two main tools: SolidWorks and ANSYS Fluent. SolidWorks was used to design the NACA 0012 airfoil geometry, including the version with a groove. It allowed for precise and accurate modeling of the airfoil profile. Meanwhile, ANSYS Fluent was used to perform computational fluid dynamics (CFD) simulations. It helped analyze the airflow around the airfoil and determine key aerodynamic parameters such as lift and drag.

2.5.1 SolidWorks Software

SolidWorks was used to design the 2D geometry of the NACA 0012 airfoil for aerodynamic analysis due to its symmetrical profile and well-known aerodynamic behavior. Coordinates for the airfoil were generated using Airfoil Tools and imported into SolidWorks, where the baseline airfoil sketch was created and extruded into a surface. This geometry was then exported in IGS format for use in ANSYS Fluent.

For the grooved configuration, the baseline sketch was duplicated, and a shallow groove was added to the airfoil surface either on the upper, lower, or both surfaces without significantly altering the overall shape. The modified geometry was also exported as an .IGS file. Both baseline and grooved models were then imported into ANSYS Design Modeler for CFD simulation preparation in ANSYS Fluent.

2.5.2 Ansys Workbench Software

This study uses ANSYS, a powerful computational fluid dynamics (CFD) software, to simulate airflow over both baseline and grooved NACA 0012 airfoils. The goal is to evaluate the aerodynamic impact of groove modifications. The simulation involves selecting appropriate turbulence models, setting boundary conditions, and applying relevant Reynolds numbers and angles of attack. A computational mesh is created, with finer elements near the groove areas to capture detailed flow features like separation, vortex formation, and reattachment. A grid independence study ensures the accuracy of results by testing various mesh densities to confirm that lift (Cl) and drag (Cd) coefficients remain consistent regardless of mesh size.

After simulation, ANSYS provides key aerodynamic data, including Cl, Cd, and pressure distribution—allowing comparison between the baseline and grooved configurations. It also generates visual outputs like streamlines and velocity contours to help analyze airflow behavior. This simulation approach ensures high-fidelity results that support informed design decisions and future aerodynamic improvements.

2.5.2.1 Ansys Workbench Software

The ANSYS Fluent workflow includes sequential steps that guide users through the process of running a computational fluid dynamics (CFD) simulation. Fig. 6 shows the steps involved for simulation development in Ansys Fluent CFD. Pre-processing (geometry preparation and meshing), solving (simulation), and post-processing (result analysis) are all steps in this approach.

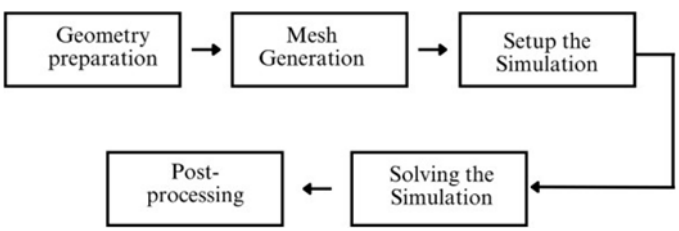

Fig. 6 *Simulation development in Ansys Fluent CFD*

Progress in Aerospace and Aviation Technology Vol. 5 No. 1 (2025) p. 55-84

2.5.2.2 Procedure of Ansys Fluent

Fig. 7 illustrates the Fluid Flow (Fluent) module within ANSYS Workbench, a comprehensive engineering simulation platform employed in this study for computational fluid dynamics (CFD) analysis. The figure depicts the integrated workflow environment, highlighting the sequential components of the simulation process, including geometry import, meshing, setup of boundary conditions and parameters (such as inlet velocity, outlet pressure, and turbulence models), solution execution, and results evaluation. First, the sketches were imported into the geometry tab to define the enclosure and object. Then, transfer to the mesh tab to create meshes for the model. After that, set up the parameters for simulation, such as inlet and outlet compartments, velocity of the object, direction of the speed, and calculation for the variables. Then, evaluate in the result tab to analyze the data for the model.

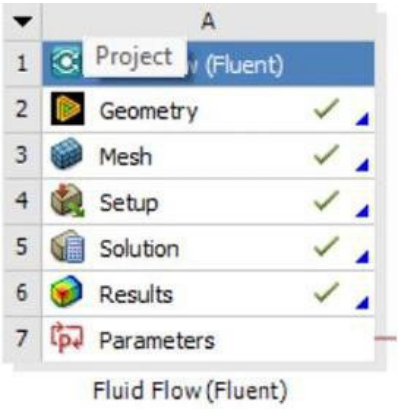

Fig. 7 *The fluid flow (fluent) module in ANSYS workbench*

2.5.2.3 Geometry

The geometry preparation begins by importing the airfoil coordinates obtained from the Airfoil Tools website into ANSYS DesignModeler (Fluent). Fig. 8 illustrates the 2D geometry setup of the NACA 0012 airfoil used for the computational fluid dynamics (CFD) simulations. These coordinates are used to reconstruct the 2D shape of the airfoil using the sketching tool on the XY plane. After the initial shape is formed, a line is drawn at the chord length to act as the axis of rotation for angle of attack (AoA) variations. Rotation is a crucial step in this project, as the airfoil will be analyzed at multiple angles, specifically at 0°, 2°, 4°, 6°, 8°, and 10°, to study the aerodynamic performance under different flow incidences.

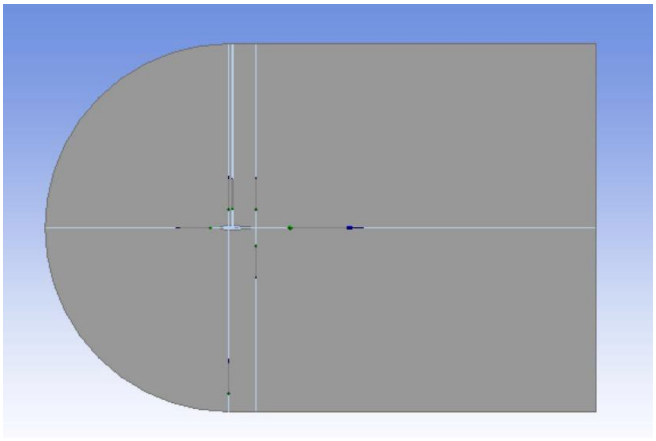

Fig. 8 *Geometry in Ansys*

To ensure better control of the simulation environment, a C-domain was constructed around the airfoil. This domain provides an appropriate far-field boundary, reducing boundary interference and better replicating freestream conditions. Additionally, a projection line is used to assist in defining boundaries and guiding mesh generation, especially when applying a structured mesh or boundary layer mesh. One important precaution taken was addressing the trailing edge gap, as imported airfoil coordinates often do not perfectly close at the trailing edge. This was manually corrected to form a watertight geometry. Finally, boundary layers will be generated

around the airfoil surface to capture the near-wall flow behavior, which is critical for observing flow separation, transition, and pressure distribution.

2.5.2.4 Mesh

As illustrated in Fig. 9, the full domain meshing within the ANSYS environment encompasses a structured or unstructured grid applied across the computational domain surrounding the NACA 0012 airfoil, including the C-domain enclosure to replicate free-stream conditions and minimize boundary interference. In this simulation, a structured mesh approach was adopted, where rectangular (hexahedral) elements are arranged in a uniform, grid-like manner. This type of mesh provides strong numerical stability and allows for more efficient computation by the CFD solver.

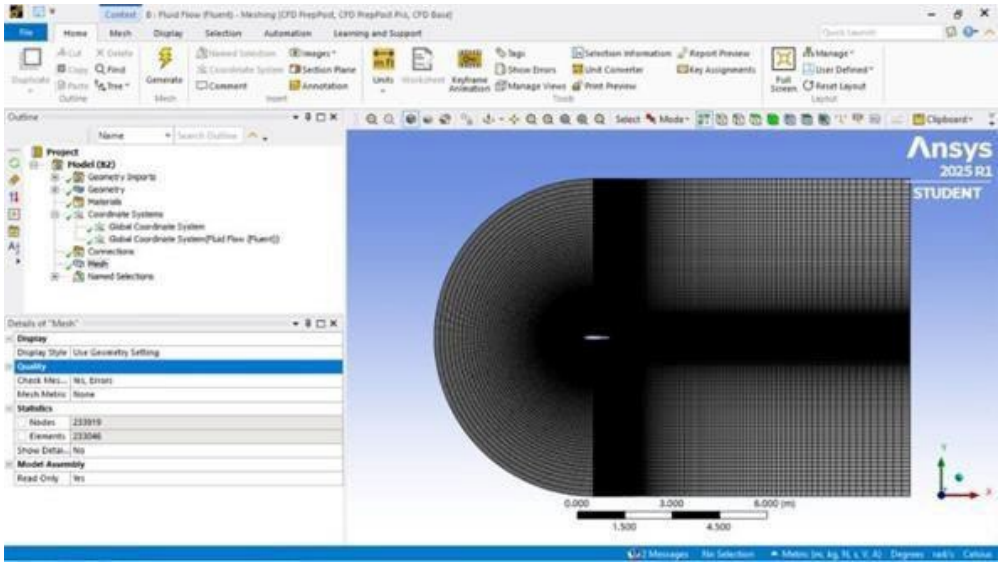

Fig. 9 *Full domain meshing in Ansys*

This study anticipates fluid flow disturbances, vortex formation, and potential separation in the groove region. Consequently, a more refined and intricate mesh was implemented in this area, utilizing an unstructured mesh with triangular elements to conform to the groove's curved geometry. Furthermore, an inflation layer technique was employed to precisely resolve boundary layer effects adjacent to the groove surface. This involved a maximum of 15 inflation layers for the boundary wall, limited to 5 layers within the groove region to adhere to the specified growth rate. Such an arrangement facilitates accurate computation of velocity and pressure gradients near the wall, essential for robust aerodynamic performance evaluation. Fig. 10 depicts the detailed meshing at the groove, highlighting these localized refinements.

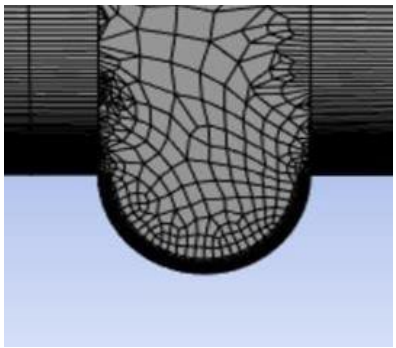

Fig. 10 *Meshing at the groove*

2.5.2.5 Setup

In this study, the simulation setup is carefully configured to accurately represent the aerodynamic behavior of the NACA 0012 airfoil. Table 4 shows the parameter setup for the simulation model. The K-omega SST turbulence model is selected due to its robustness in predicting flow separation and near-wall behavior, which is crucial for capturing the effect of grooves on airflow. The solver used is density-based, suitable for compressible flow

Progress in Aerospace and Aviation Technology Vol. 5 No. 1 (2025) p. 55-84

conditions even at low Mach numbers. The velocity formulation is set to absolute, and the simulation is treated as steady-state in a 2D planar domain to reduce computational cost while maintaining accuracy. The working fluid in this simulation is air, defined with standard properties such as density (1.225 kg/m^3), specific heat (Cp = 1006.43 J/kg·K), thermal conductivity (0.0242 W/m·K), and viscosity (1.789 × 10^{-5} kg/m·s). The simulation domain includes three boundary conditions: pressure far-field at the free stream, velocity inlet, and pressure outlet. At the inlet, a uniform velocity of 43.9 m/s is applied with turbulence modeled using a turbulent viscosity ratio of 1. The outlet and free-stream conditions are set with zero gauge pressure, and the direction of flow components is defined accordingly to represent the actual aerodynamic flow over the airfoil. Mesh quality and boundary conditions are carefully defined to ensure convergence and numerical stability, especially when simulating the grooved configurations of the air.

Table 4 *Parameter setup for the model*

Setup		
Model	K omega	
Solver	Density-Based	
Velocity Formulation	Absolute	
Time	Steady	
2D space	Planar	
Model		
Model	K Omega	SST
Material selection		
Air	Density (kg/m^3) = 1.225 Cp (specific heat) = 1006.43 j/kg-k	Thermal conductivity = 0.0242 w/m-k Viscosity = 1.789e-5 kg/m-s
Boundary condition		
Free	Type: Pressure far field Gauge Pressure = 0 Mach Number = 0	x-component of flow direction = 1 y y-component of flow direction = 0
Inlet	Type: Velocity inlet Velocity Specification Method = Magnitude and direction Reference Frame = Absolute Velocity Magnitude = 43.9 m/s Turbulence	Supersonic/initial gauge pressure = 0 Pa X-component of flow direction = 1 Y-component of flow direction = 0 Specification method = Turbulent Viscosity Ratio Turbulent Viscosity Ratio = 1
Outlet	Type: pressure outlet Gauge Pressure = 0 Pa Backflow direction specification Method = Normal to Boundary	Specification Method: Turbulent Viscosity Ratio Backflow Turbulent Viscosity ratio = 1 Turbulence

2.5.2.6 Solution

The solution method is set to a coupled pressure-velocity scheme, which provides improved convergence for compressible flow problems. For spatial discretization, second-order upwind schemes are used for both flow and modified turbulent viscosity to achieve higher accuracy in capturing gradients near the wall and in the flow field. The gradient calculation is done using the least-squares cell-based method, which helps in maintaining consistency in structured and unstructured meshes.

Solution control parameters such as under-relaxation factors are set to their standard values, with the turbulent viscosity modified to 0.75 for better convergence. The Courant number is set to 5 to control the time step in the steady-state solver.

To monitor the simulation performance, drag and lift coefficients are tracked at the airfoil wall zones. The results are printed and plotted during the simulation to observe convergence behavior and flow stability. The hybrid initialization method is chosen to start the solution using estimated flow conditions from the inlet, which improves the convergence rate for complex geometries.

Initial conditions are set for pressure (0 pa), temperature (300 k), and velocity components (x = 43.9 m/s, y = 0 m/s), with the reference frame relative to the cell zone. The number of iterations is fixed at 500 to ensure that the residuals and force monitors reach a stable and converged state.

Table 5 *Solution method*

Solution Method		
Model	K Omega	
Pressure-velocity coupling	Scheme: coupled	
Special discretization		
Gradient	Least squares cell-based	
Flow	Second-order upwind	
Modified Turbulent viscosity	Second-order upwind	
Solution control		Modified turbulent viscosity = 0.75
Courant number: 5		Turbulent viscosity = 1
Under relaxation factor:		Solid = 1
Monitors		
Residual and force monitor	Create: Drag coefficient Wall zones: airfoil Option: Print to console and plot Force vector: X=1, Y=0	Create: lift coefficient Wall zones: airfoil Option: Print to console and plot Force vector: X=0, Y=1
Solution initialization		
Method	Hybrid initialization	
Compute from	Inlet	
Ref. frame	Relative to the cell zone	
Initial values	Gauge pressure (Pa) = 0 T(K)=300	X velocity (m/s) = 43.9 Y velocity (m/s) = 0
Run calculation		
Number of iterations = 500		

2.5.2.7 Result

The lift and drag coefficient can be obtained by clicking the parameter tab, as shown in Fig. 11. It can be shown in the parameter because it has been set up to create a parameter for the lift and drag coefficient. To extract the pressure coefficient (Cp) data for validation purposes, the XY Plot tool in Ansys Fluent was used. Fig. 12 shows the Ansys Fluent XY plot tool settings for extracting pressure coefficients. The surface of the baseline airfoil was selected, with the X-axis set to the direction vector and the Y-axis set to the pressure coefficient. Node values were activated, and the output was written to a file for further comparison with published benchmark data. This setup enabled accurate Cp plotting along the airfoil surface, which was essential for validating simulation accuracy.

Progress in Aerospace and Aviation Technology Vol. 5 No. 1 (2025) p. 55-84

Outline of All Parameters

	A	B	C	D
1	ID	Parameter Name	Value	Unit
2	Input Parameters			
3	Fluid Flow (Fluent) (A1)			
4	P1	AoA	0	degree
*	New input parameter	New name	New expression	
6	Output Parameters			
7	Fluid Flow (Fluent) (A1)			
8	P2	drag-op	0.0091593	
9	P3	lift-op	0.00068413	
10	Fluid Flow (Fluent) (B1)			
11	P5	Lift coefficient	0.21497	
12	P6	Drag Coefficient	0.0094792	
13	Fluid Flow (Fluent) (C1)			
14	P9	drag-op	0.011808	
15	P10	lift-op	0.63909	
16	Fluid Flow (Fluent) (D1)			
17	P13	drag-op	0.016791	
18	P14	lift-op	1.042	
19	Fluid Flow (Fluent) (E1)			
20	P7	drag-op	0.010354	
21	P8	lift-op	0.42837	
22	Fluid Flow (Fluent) (F1)			
23	P11	drag-op	0.01378	
24	P12	lift-op	0.8538	

Fig. 11 *Data for lift coefficient and drag coefficient*

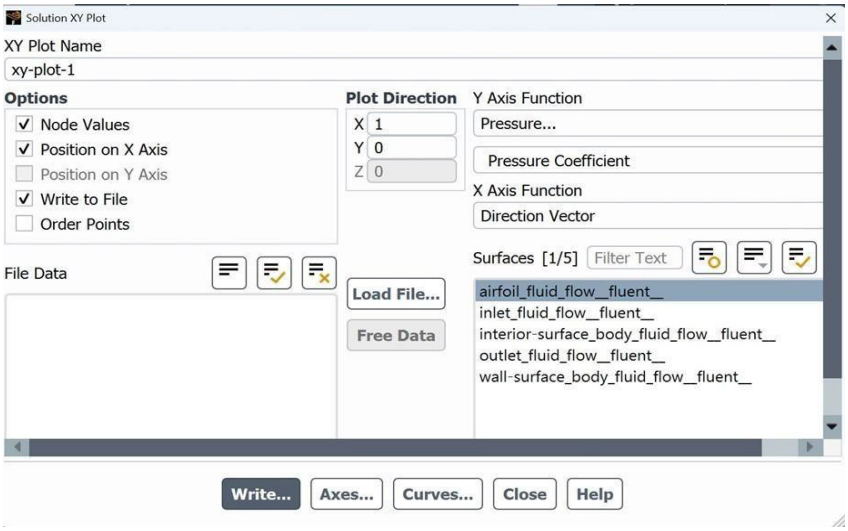

Fig. 12 *Ansys Fluent XY Plot settings for extracting pressure coefficient (Cp) along the airfoil surface for validation purposes*

3. Results and Discussion

This section summarizes the CFD results for both baseline and grooved NACA 0012 airfoils at low angles of attack (0°–10°), aiming to assess the impact of different groove placements on aerodynamic performance. It begins with model validation and a grid independence test to ensure simulation accuracy. Various groove sizes are tested to identify the optimal one, which is then used in multiple configurations. Key aerodynamic parameters—lift, drag,

and Cl/Cd ratio—are analyzed for each setup, supported by flow visualizations. The section ends with a comparative evaluation, identifying the most effective groove design for improving performance over the baseline.

3.1 Validation

Table 6 presents the validation of the simulated lift coefficient (Cl) results against experimental data for the NACA 0012 airfoil, obtained from Abbott and Doenhoff [9]. This comparison is essential to evaluate the accuracy of the CFD model used in the simulation. The experimental and simulation values are compared across various angles of attack (AOA), and both the absolute and percentage errors are calculated. According to common CFD validation standards, an error margin within 10% is generally considered acceptable for aerodynamic simulations involving experimental comparison. Since all available simulation data in Table 6 falls well within this range, the results are deemed valid. Therefore, the current CFD setup is considered sufficiently accurate and reliable for further aerodynamic analysis of the NACA 0012 airfoil, including studies involving groove modifications.

Table 6 *Comparison of experimental and simulation lift coefficient (Cl) for NACA 0012 airfoil*

No.	Angle of Attack (°)	Cl Experimental	Cl Simulation	Error	Error Percentage
1	0.00000	0.00000	0.00000	0.00000	0.00%
2	0.94001	0.12061	0.11711	0.02903	2.90%
3	1.96944	0.21553	0.21415	0.00641	**0.64%**
4	2.99515	0.34477	0.32104	0.06882	6.88%
5	3.85131	0.43960	0.42751	0.02749	2.75%
6	4.87888	0.55168	0.53330	0.03332	3.33%
7	5.90831	0.64660	0.63808	0.01318	1.32%
8	7.96346	0.87076	0.84319	0.03166	3.17%
9	10.18910	1.12074	1.03937	0.07261	**7.26%**
10	11.04710	1.19842	1.13178	0.05561	5.56%
13	16.56780	1.42443	1.45853	0.02394	2.39%

Fig. 13 compares the lift coefficient (Cl) versus angle of attack (AoA) for the NACA 0012 airfoil using CFD simulation results and experimental data from Abbott and Doenhoff [9]. Both show a similar trend, with Cl increasing linearly up to about 14°–16°, indicating good agreement in the pre-stall region. The maximum Cl occurs around 16° AoA, marking the stall point where lift drops sharply due to flow separation. The experimental data peaks higher at around 1.6, while the simulation reaches about 1.45, with a steeper decline reflecting CFD's limitations in modeling post-stall behavior accurately.

Fig. 13 *Graph of Cl difference vs. angle of attack for experimental and simulation NACA 0012*

3.2 Grid Independent Test

For each mesh configuration, simulations were conducted across several angles of attack (AOA), and the corresponding lift and drag coefficients were recorded. The results are presented in Table 7 and Table 8. These mesh densities provided sufficient resolution, especially near the airfoil surface, and included 15 inflation layers

to accurately resolve the boundary layer, which is critical for analyzing flow separation and pressure distribution. The overall simulation results, regardless of the number of nodes, demonstrate only minor variations. This test showed that the number of nodes within the range of 60450 and 136730 does not affect the result of the simulation. In conclusion, the Grid Independence Test successfully confirmed that the simulation results are mesh-independent and reflect true physical behavior, thereby enhancing the credibility and robustness of the CFD study.

Table 7 *Lift coefficient (Cl) vs. angle of attack (AOA) for different mesh densities*

	Lift coefficient (Cl)		
AOA	**136730**	**92390**	**60450**
0	0.00000	0.00000	0.00000
2	0.21458	0.21450	0.21415
4	0.42830	0.42819	0.42751
6	0.63951	0.63938	0.63808
8	0.84585	0.84565	0.84320
10	1.04400	1.04360	1.03940

Table 8 *Drag coefficient (Cd) vs. angle of attack (AOA) for different mesh densities*

	Drag coefficient (Cd)		
AOA	**136730**	**92390**	**60450**
0	0.00912	0.00910	0.00909
2	0.00939	0.00938	0.00937
4	0.01012	0.01020	0.01021
6	0.01158	0.01159	0.01167
8	0.01360	0.01364	0.01384
10	0.01640	0.01646	0.01685

3.3 Analysis for Different-Size Grooves

This subsection presents an analysis of the effect of different groove sizes on the aerodynamic performance of the airfoil. The purpose of this analysis is to determine the most appropriate groove size that can be applied consistently across all design configurations. The grooves are positioned at a fixed location of 0.25C on the upper surface, and three different sizes are tested: 0.5 cm, 1.0 cm, and 1.5 cm. Assuming a chord length of 1 meter (1C = 1 m), these correspond to groove-to-chord length ratios of 0.005C, 0.010C, and 0.015C, respectively. This ratio-based comparison ensures consistency in evaluating aerodynamic influence at different scales. By examining how each groove size affects lift and drag characteristics, this study aims to identify the optimal dimension that enhances flow control while minimizing aerodynamic penalties.

3.3.1 Lift Coefficient Analysis for Different Grooves Sizes

This subsection focuses on how different groove sizes affect the lift-generating capability of the airfoil. The grooves are positioned at a fixed location of 0.25C on the upper surface, and three sizes are tested: 0.5 cm (0.005C), 1.0 cm (0.010C), and 1.5 cm (0.015C), based on a chord length of 1 meter. The purpose of this analysis is not only to observe how each size influences lift performance across varying angles of attack but also to identify the most effective groove size that can be used consistently in subsequent design evaluations. The groove size that offers the greatest lift enhancement with stable behavior will be selected for further analysis in the following sections.

Fig. 14 shows the comparison of lift coefficient Cl against angle of attack (AOA) for different groove diameters and the NACA0012 baseline. Table 9 presents the lift coefficient error and percentage difference compared to the NACA0012 baseline. Based on the Cl data results, the 0.5 cm groove diameter shows minimal differences across all angles of attack (AOA), indicating that it has very little impact on lift performance. The Cl changes are mostly close to zero, with percentage differences below ±0.2%, suggesting that this groove size maintains lift characteristics similar to the baseline. For the 1.0 cm groove, a more noticeable improvement is observed, particularly at AOA 6° and 10°, where the lift increases by 2.47% and 2.14%, respectively. This indicates that the 1.0 cm groove can enhance lift under certain flow conditions. In contrast, the 1.5 cm groove generally results in

negative Cl differences at almost all AOAs, implying a reduction in lift performance as groove size increases beyond 1.0 cm.

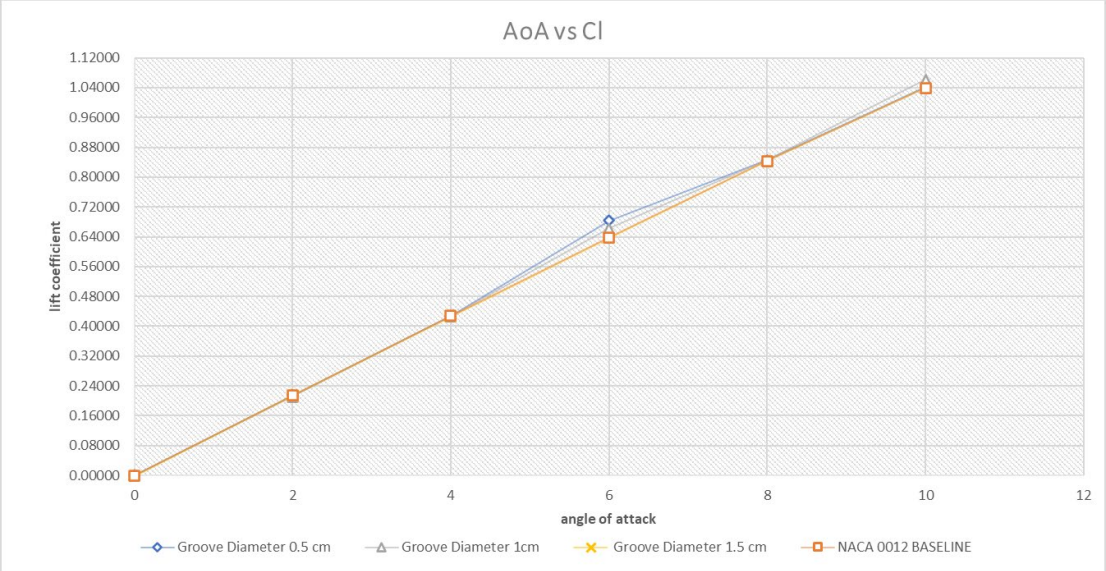

Fig. 14 *Graph of Cl difference vs. angle of attack for each groove diameter and NACA 0012 baseline*

Table 9 *Lift coefficient error and percentage difference compared to baseline for various groove diameters across different angles of attack*

	0.5 cm diameter		1.0 cm diameter		1.5 cm diameter	
AOA	**Cl Increment**	**Percentage Increment**	**Cl increment**	**Percentage Increment**	**Cl increment**	**Percentage Increment**
0	-0.00003	0.00%	0.00022	0.02%	-0.00116	-0.12%
2	-0.00042	-0.20%	-0.00275	-0.28%	-0.00138	-0.14%
4	-0.00005	-0.01%	-0.00061	-0.06%	-0.00155	-0.16%
6	0.00010	0.02%	0.02473	2.47%	-0.00102	-0.10%
8	0.00131	0.16%	0.00193	0.19%	-0.00035	-0.03%
10	0.00234	0.22%	0.02140	2.14%	-0.00025	-0.03%

3.3.2 Drag Coefficient Analysis for Different Grooves Sizes

This subsection evaluates the effect of groove size on aerodynamic drag. Using the same groove location and sizes as in the lift analysis, the focus is on how each dimension influences the drag coefficient (Cd) at different angles of attack. While larger grooves may enhance flow control, they can also increase surface disturbance and drag. Therefore, this analysis is essential in determining which groove size provides an acceptable trade-off between maintaining low drag and achieving aerodynamic improvements. The selected groove size from this evaluation will be applied in all subsequent groove configuration analyses to ensure consistency and optimal aerodynamic performance.

Fig. 15 shows the Cd data against angle of attack (AOA) for all groove sizes and the NACA0012 baseline. Table 10 presents the drag coefficient increment and percentage increment compared to the NACA0012 baseline. All groove sizes show very small differences in terms of drag coefficient increments, typically ranging from −0.15% to +0.02%, indicating that the grooves have a minimal effect on drag. The 0.5 cm and 1.5 cm grooves generally result in a slight increase in drag or very minimal changes. The 1.0 cm groove shows a small reduction in drag at higher AOAs, especially at AOA 10°, where drag decreases by 0.15%. Although this reduction is minor, it suggests that the 1.0 cm groove may offer a slight aerodynamic advantage by reducing drag at specific operating conditions.

Progress in Aerospace and Aviation Technology Vol. 5 No. 1 (2025) p. 55-84

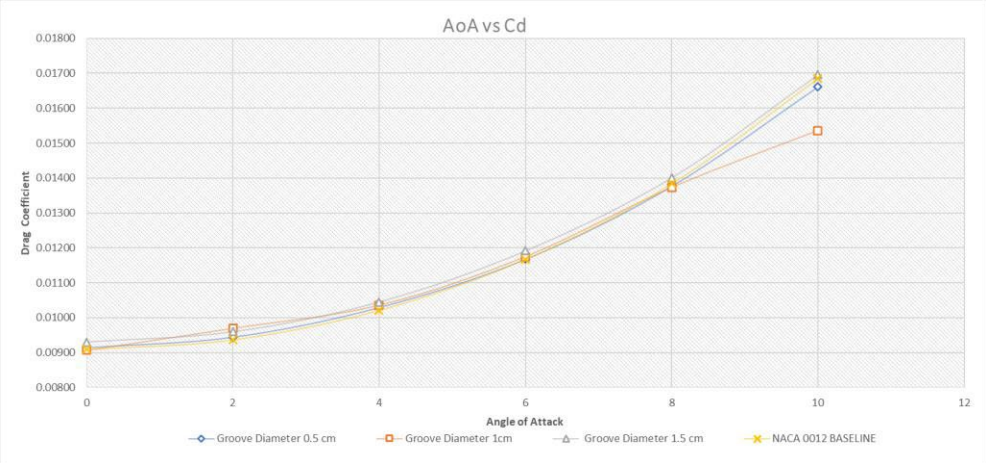

Fig. 15 *Graph of Cd Difference vs. Angle of Attack for Each Groove Diameter and NACA 0012 baseline*

Table 10 *Drag coefficient increment and percentage increment compared to baseline for various groove diameters across different angles of attack*

	0.005C Diameter		0.01C Diameter		0.015C Diameter	
AOA	**Cd Increment**	**Percentage Increment**	**Cd Increment**	**Percentage Increment**	**Cd Increment**	**Percentage Increment**
0	0.00007	0.01%	-0.00002	0.00%	0.00021	0.02%
2	0.00011	0.01%	0.00033	0.03%	0.00023	0.02%
4	0.00011	0.01%	-0.00011	-0.01%	0.00024	0.02%
6	0.00003	0.00%	0.00008	0.01%	0.00024	0.02%
8	-0.00004	0.00%	-0.00011	-0.01%	0.00017	0.02%
10	-0.00019	-0.02%	-0.00149	-0.15%	0.00011	0.01%

Taking both lift and drag performance into account, the 1.0 cm groove diameter provides the best overall aerodynamic performance. It offers improved lifts at key AOAs while showing a small drag reduction at higher angles. The 0.5 cm groove shows stable but unremarkable results, with performance very close to the baseline. Meanwhile, the 1.5 cm groove tends to reduce lift slightly without providing any meaningful drag benefit. The 1.0 cm groove is therefore the most successful in increasing aerodynamic efficiency out of the three tested groove sizes. Based on these findings, the 1.0 cm groove diameter is selected to be used for the next stage of analysis involving the NACA 0012 airfoil with groove configurations.

3.4 Parallel Groove Configuration

In this section, we investigate the aerodynamic performance of three different parallel groove configurations on the NACA 0012 airfoil. The grooves are positioned along the chord length I at three different locations: 0.20C, 0.25C, and 0.30C from the leading edge. These configurations are designed to evaluate how the position of the groove affects lift and drag characteristics, as well as overall aerodynamic efficiency.

3.4.1 Lift Coefficient Analysis for Parallel Groove

In this subsection, the lift coefficient (Cl) for each groove configuration is compared across several angles of attack (AOA). Fig. 16 and Table 11 show the lift coefficient (Cl) for parallel groove positions and the NACA0012 baseline at different AOAs. The results are analyzed to observe any improvements or changes in lift compared to the baseline airfoil. Although the differences are relatively small, the data shows how groove placement affects lift generation. The lift performance for the parallel groove configurations (0.20C, 0.25C, and 0.30C) shows a consistent trend across increasing angles of attack (AOA). All three configurations produce lift coefficients very close to the baseline (NACA 0012), with only minimal variations. At low AOA (0°–4°), the differences are almost negligible, indicating that groove placement has a limited effect on lift at these angles. However, as the AOA increases (especially at 8° and 10°), the configuration with the groove at 0.30C shows slightly higher Cl values compared to others, reaching 1.0409 at 10°, which is marginally higher than the baseline (1.03937). The differences between the parallel designs are small, but this slight improvement at higher AOA suggests that placing

the groove further aft (at 0.30C) may enhance suction and delay flow separation, contributing to better lift generation under higher loading conditions.

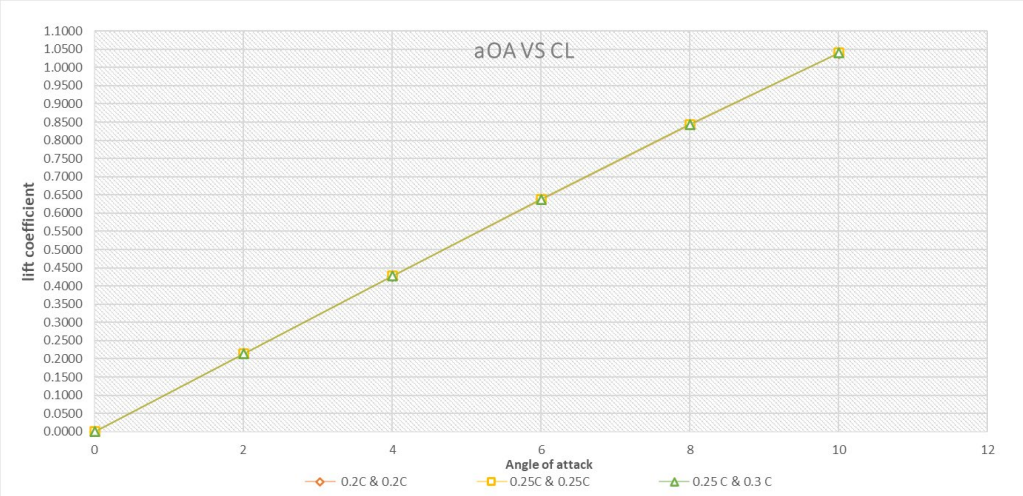

Fig. 16 *Lift Coefficient (Cl) vs. angle of attack (AoA) for different parallel groove positions and NACA 0012 baseline*

Table 11 *Lift coefficient (Cl) for parallel groove positions on NACA and baseline*

	Lift Coefficient (Cl)			
AOA	**Parallel 0.20 C**	**Parallel 0.25 C**	**Parallel 0.30 C**	**Baseline**
0	0.00024	0.00005	0.00015	0.00000
2	0.21366	0.21369	0.21410	0.21415
4	0.42658	0.42686	0.42720	0.42751
6	0.63694	0.63746	0.63779	0.63808
8	0.84236	0.84291	0.84323	0.84319
10	1.03890	1.03992	1.04090	1.03937

3.4.2 Drag Coefficient Analysis for Parallel Groove

Fig. 17 and Table 12 present the drag coefficient (Cd) values for the three parallel groove configurations as well as the NACA0012 baseline. The analysis focuses on identifying whether the grooves contribute to a reduction or increase in drag at various AOAs. Any changes in Cd, even small ones, are important as they directly influence the aerodynamic efficiency of the airfoil. Drag behavior shows more noticeable differences compared to lift. All parallel groove configurations result in slightly higher drag coefficients than the baseline, especially as AOA increases. At 0°, the drag coefficients for the groove cases are between 0.00927 and 0.00933, slightly above the baseline (0.00909). As AOA increases, the drag values for all configurations rise accordingly, with Parallel 0.25C showing the highest drag throughout, reaching 0.01696 at 10°. Parallel 0.30C, while providing the best lift, still maintains a slightly lower drag than 0.25C, with 0.01689 at 10°. The baseline maintains the lowest drag at nearly every AOA. These results suggest that while parallel grooves have minimal lift benefit, they introduce a small but consistent drag penalty. The 0.30C configuration offers the best trade-off, slightly improved lift with relatively controlled drag.

Progress in Aerospace and Aviation Technology Vol. 5 No. 1 (2025) p. 55-84

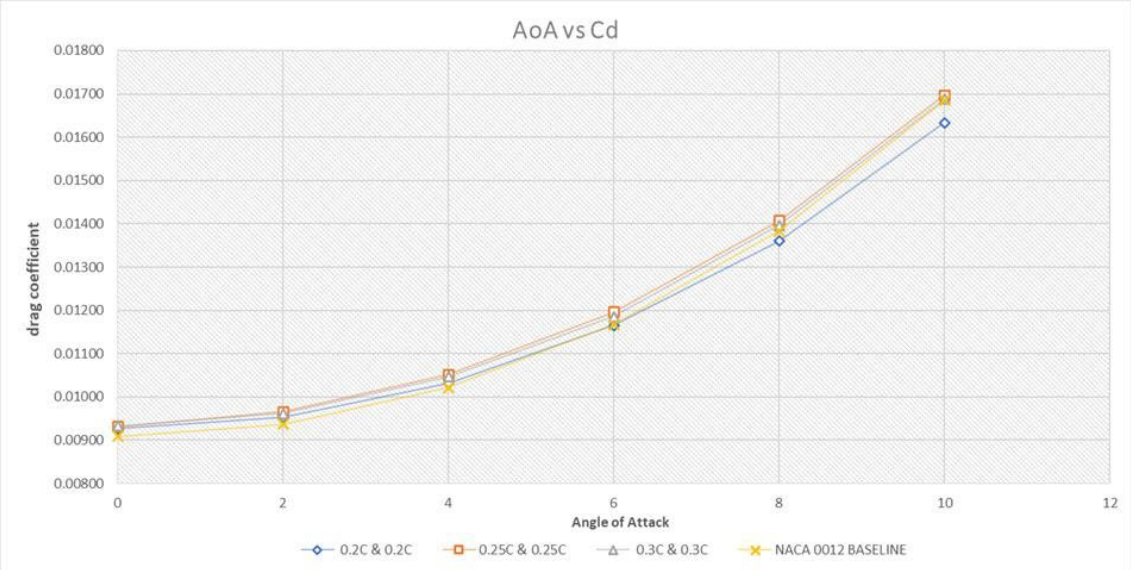

Fig. 17 *Drag coefficient (Cd) vs. angle of attack (AoA) for different parallel groove positions and NACA 0012 baseline*

Table 12 *Drag coefficient (Cd) for parallel groove positions on NACA and baseline*

	Drag Coefficient			
AOA	**Parallel 0.20C**	**Parallel 0.25C**	**Parallel 0.30C**	**Baseline**
0	0.00927	0.00931	0.00933	0.00909
2	0.00953	0.00966	0.00962	0.00937
4	0.01032	0.01051	0.01047	0.01021
6	0.01165	0.01196	0.01186	0.01167
8	0.01360	0.01407	0.01397	0.01384
10	0.01634	0.01696	0.01689	0.01685

3.4.3 Comparison and Selection

Based on the lift and supporting drag data, this subsection identifies the most suitable groove configuration. The selection is primarily based on the configuration that produces the highest or most stable lift, while drag is taken into account to ensure aerodynamic balance. If lift improvement is minor and drag increase is substantial, the baseline may still be considered optimal.

Table 13 presents the lift coefficient (Cl) differences between three parallel groove configurations positioned at 0.20C, 0.25C, and 0.30C and the baseline NACA 0012 airfoil. The data shows that the variations in Cl across all angles of attack (AOA) are relatively small, typically within ± 0.1%. The grooves at 0.20C and 0.25C generally exhibit slightly lower Cl values compared to the baseline, particularly noticeable at mid-range AOAs (4° to 8°), where flow separation effects start to become more pronounced. This suggests that these two groove positions may slightly disrupt the airflow or provide no lift advantage under these conditions.

Table 13 *Lift coefficient (Cl) increment and percentage increment for parallel groove configurations compared to baseline*

	0.2C & 0.2C		0.25C & 0.25C		0.30C & 0.30C	
AOA	**Cl Increment**	**Percentage Increment**	**Cl Increment**	**Percentage Increment**	**Cl Increment**	**Percentage Increment**
0	0.00024	0.02%	0.00005	0.00%	0.00015	0.02%
2	-0.00049	-0.05%	-0.00046	-0.05%	-0.00005	-0.01%
4	-0.00093	-0.09%	-0.00065	-0.07%	-0.00031	-0.03%
6	-0.00114	-0.11%	-0.00062	-0.06%	-0.00029	-0.03%
8	-0.00083	-0.08%	-0.00028	-0.03%	0.00004	0.00%
10	-0.00047	-0.05%	0.00055	0.06%	0.00153	0.15%

The drag coefficient (Cd) differences shown in Table 14 are also relatively minor, with most values falling within ± 0.03% when compared to the baseline. This indicates that the introduction of parallel grooves does not significantly increase the surface drag. Among the three configurations, the 0.20C groove exhibits a slight advantage in drag reduction, particularly at AOA 10°, where a Cd reduction of -0.00051 (-0.05%) is observed, the most notable drag improvement recorded in the study. This could be due to a slight delay in flow separation or a reduction in turbulent wake effects at that groove position.

Table 14 *Drag coefficient (Cd) increment and percentage increment for parallel groove configurations compared to baseline*

	0.2C & 0.2C		0.25C & 0.25C		0.30C & 0.30C	
AOA	**Cd Increment**	**Percentage Increment**	**Cd Increment**	**Percentage Increment**	**Cd Increment**	**Percentage Increment**
0	0.00018	0.02%	0.00022	0.02%	0.00025	0.02%
2	0.00016	0.02%	0.00029	0.03%	0.00025	0.03%
4	0.00010	0.01%	0.00030	0.03%	0.00025	0.03%
6	-0.00002	0.00%	0.00029	0.03%	0.00019	0.02%
8	-0.00023	-0.02%	0.00023	0.02%	0.00013	0.01%
10	-0.00051	-0.05%	0.00012	0.01%	0.00004	0.00%

Considering both lift and drag, the 0.30C groove is the most favorable configuration. It consistently improves lift, especially at higher angles of attack, without causing a significant drag increase, maintaining overall aerodynamic efficiency. Although the 0.20C groove slightly reduces drag, it shows lower lift performance than the baseline. The 0.25C groove also offers minimal benefit. Hence, 0.30C is selected as the most suitable groove position for further aerodynamic analysis.

3.5 Fixed Upper Groove (0.25C) and Variable Lower Position

This section investigates the aerodynamic performance of fixed groove configurations on the NACA 0012 airfoil, where the upper groove position is fixed at 0.25 C, and the lower groove position is varied across four designs: 0.25 C, 0.30 C, 0.35 C, and 0.40 C. Unlike the earlier parallel groove design, these configurations introduce two grooves on the airfoil surface, one on the suction side's upper surface and one on the lower surface, with the intent of modifying boundary layer behavior. The fixed groove on the 0.25 C upper surface is placed to influence the suction-side flow by enhancing energy near the surface, which may help delay separation and improve lift. Meanwhile, the variation in lower groove placement is designed to assess how different downstream positions affect pressure distribution and drag. The overall goal of these configurations is to determine whether this upper-lower groove combination can provide aerodynamic improvements over the baseline airfoil, particularly in lift generation and drag control.

Fig. 18 and Table 15 present the lift coefficient data for different fixed upper groove configurations. The lift coefficient (Cl) data across various angles of attack (AOA) for the NACA 0012 airfoil equipped with different dual-groove configurations reveals consistent aerodynamic trends. In all cases, the Cl increases with AOA, as expected for a symmetrical airfoil. Among the tested configurations, the dual groove placed at 0.25C & 0.40C consistently shows the highest Cl values across all AOAs, indicating improved aerodynamic performance. At low angles such as 0° and 2°, the impact of the grooves is minimal, but a slight increase in Cl is still observed compared to the baseline, suggesting early boundary layer influence. As the AOA increases to 4°, 6°, and 8°, the advantages of more groove placements become more evident, with 0.25C & 0.40C outperforming other designs. This trend continues at 10°, where this configuration achieves the highest lift coefficient (Cl = 1.042), slightly surpassing both the baseline and other groove placements. Overall, positioning the second groove further downstream appears to be more effective in energizing the flow and delaying separation, resulting in a modest yet consistent lift enhancement across the tested range.

Progress in Aerospace and Aviation Technology Vol. 5 No. 1 (2025) p. 55-84

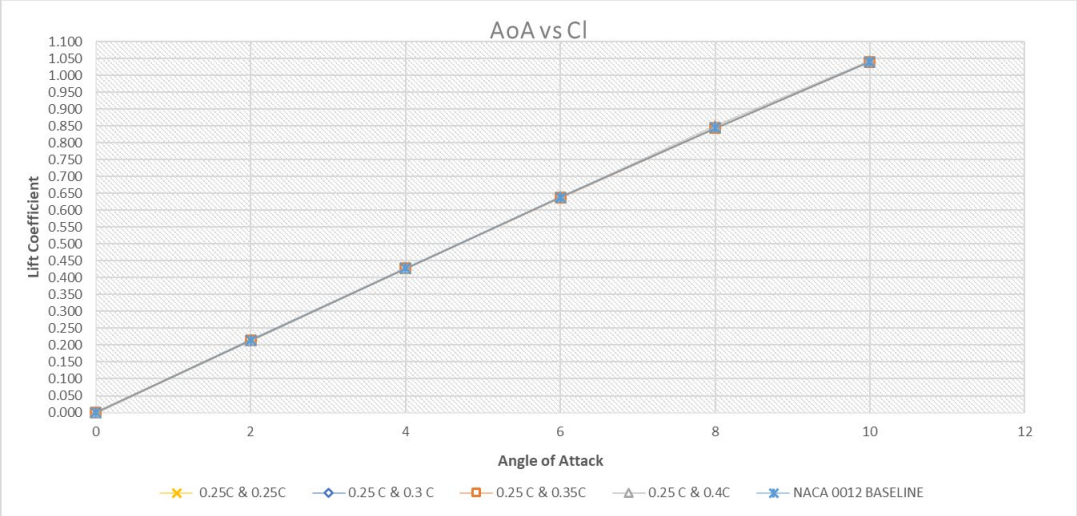

Fig. 18 *Lift coefficient (Cl) vs. angle of attack (AoA) for different parallel groove positions and NACA 0012 baseline*

Table 15 *Lift coefficient (Cl) vs. angle of attack (AOA) for different fixed upper 0.25 groove configurations and NACA0012 baseline*

	Lift coefficient				
AOA	**0.25 C & 0.25 C**	**0.25 C & 0.30 C**	**0.25 C & 0.35 C**	**0.25 C & 0.40 C**	**Baseline**
0	0.00005	0.00015	0.00039	0.00068	0.00000
2	0.21369	0.21410	0.21435	0.21497	0.21415
4	0.42686	0.42720	0.42786	0.42837	0.42751
6	0.63746	0.63779	0.63718	0.63910	0.63808
8	0.84291	0.84323	0.84338	0.84977	0.84319
10	1.03992	1.04020	1.04040	1.04200	1.03937

3.5.1 Drag Coefficient Analysis for Fixed Upper Groove (0.25C)

Fig. 19 and Table 16 display the drag coefficient results for various fixed upper groove (0.25C) configurations. The drag coefficient (Cd) increases consistently with the angle of attack (AOA) for all configurations, including the baseline case. At AOA = 0°, all grooved designs show slightly higher drag compared to the baseline, but the configuration with grooves at 0.25C & 0.40C records the lowest drag among the modified cases (Cd = 0.00916), only marginally higher than the baseline value (Cd = 0.00909). As the AOA increases to 2° and 4°, the differences between the designs become more noticeable, with the 0.25C & 0.40C configuration consistently demonstrating lower drag values. This suggests that placing the second groove further downstream contributes to improved boundary layer control, helping to reduce early flow separation and associated drag. At higher angles of attack, 6°, 8°, and 10°, this trend continues, with the 0.25 C & 0.40 C configuration maintaining the lowest drag across nearly all conditions. At AOA = 10°, this design even achieves a lower drag coefficient (Cd = 0.01679) than the baseline (Cd = 0.01685), indicating its potential to not only stabilize the flow but also reduce overall aerodynamic resistance under more demanding conditions. In contrast, configurations with closely spaced grooves (0.25C & 0.25C) produce the highest drag values, implying less effective flow management. Overall, the results indicate that fixing the upper groove at 0.25C and placing the second groove further at specifically 0.40C offers a tangible aerodynamic advantage by reducing drag and enhancing the airfoil's overall performance.

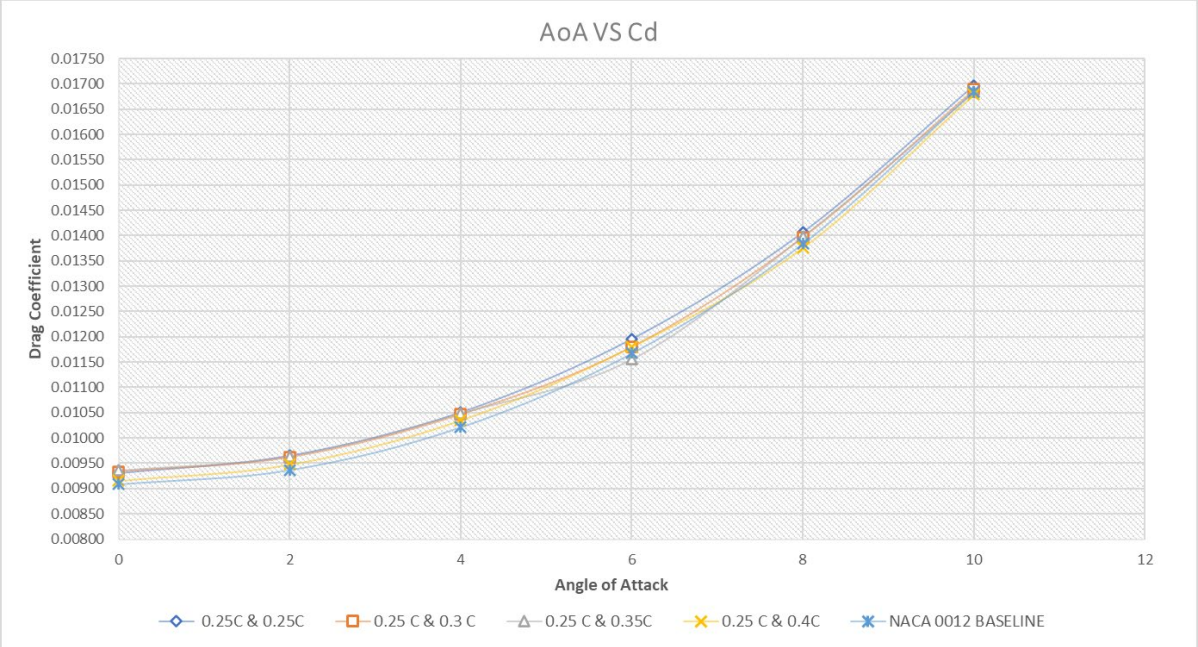

Fig. 19 *Drag coefficient (Cd) vs. angle of attack (AOA) for different parallel groove positions (0.25C) and NACA 0012 baseline*

Table 16 *Drag coefficient (Cd) vs. angle of attack (AOA) for different fixed upper groove (0.25C) configurations and NACA 0012 baseline*

	Drag coefficient				
AOA	**0.25 C & 0.25 C**	**0.25 C & 0.30 C**	**0.25 C & 0.35 C**	**0.25 C & 0.40 C**	**Baseline**
0	0.00931	0.00933	0.00936	0.00916	0.00909
2	0.00966	0.00962	0.00964	0.00948	0.00937
4	0.01051	0.01047	0.01049	0.01035	0.01021
6	0.01196	0.01180	0.01156	0.01181	0.01167
8	0.01407	0.01397	0.01398	0.01376	0.01384
10	0.01696	0.01689	0.01684	0.01679	0.01685

3.5.2 Comparison and Selection

This subsection presents a comparative analysis of lift and drag coefficient differences between the baseline NACA 0012 airfoil and fixed upper surface 0.25 C and various lower configurations. The aim is to evaluate how the placement of surface grooves at different chordwise positions affects aerodynamic performance across a range of angles of attack (AOA). Differences and percentage changes in lift (Cl) and drag (Cd) coefficients are calculated to assess the effectiveness of each design. By quantifying the impact of groove locations, this analysis helps identify the most aerodynamically efficient configuration, balancing lift enhancement with minimal drag penalties.

Table 17 shows the lift performance data at various groove configurations compared to baseline. From the drag data, the 0.25C & 0.40C configuration stands out by producing the lowest drag increase or even drag reduction compared to the baseline. At higher AOAs, especially 8° and 10°, this design achieves Cl increases of 0.66% and 0.26%, respectively, compared to the baseline. Other configurations like 0.25C & 0.25C and 0.25C & 0.30C show either small gains or slight decreases in Cl, especially at mid-range AOAs. Therefore, the groove placement (at 0.40C) appears to have the most positive influence on lift generation.

Progress in Aerospace and Aviation Technology Vol. 5 No. 1 (2025) p. 55-84

Table 17 *Lift coefficient (Cl) increment and percentage increment compared to baseline*

	0.25C & 0.25C		0.25 C & 0.3 C		0.25 C & 0.35C		0.25 C & 0.4C	
AOA	Cl Increment	Percentage Increment	Cl Increment	Percentage Increment	Cl Increment	Percentage Increment	Cl Increment	Percentage Increment
0	0.00005	0.00%	0.00015	0.02%	0.00039	0.04%	0.00069	0.07%
2	-0.00046	-0.05%	-0.00005	-0.01%	0.00020	0.02%	0.00082	0.08%
4	-0.00065	-0.07%	-0.00031	-0.03%	0.00035	0.03%	0.00086	0.09%
6	-0.00062	-0.06%	-0.00029	-0.03%	-0.00090	-0.09%	0.00102	0.10%
8	-0.00028	-0.03%	0.00004	0.00%	0.00019	0.02%	0.00658	0.66%
10	0.00055	0.06%	0.00083	0.08%	0.00103	0.10%	0.00263	0.26%

Table 18 shows the drag coefficient data at various groove configurations compared to the baseline. From the drag data, the 0.25C & 0.40C designs again stand out by producing the lowest drag increase or even drag reduction compared to the baseline. At higher AOAs, such as 8° and 10°, it shows negative drag differences, indicating actual drag reduction. Meanwhile, other configurations, especially 0.25C & 0.25C and 0.25C & 0.30C, consistently exhibit higher drag increases of around 0.02% to 0.03% across all AOAs, making them less desirable from a drag standpoint.

Table 18 *Drag coefficient (Cd) increment and percentage increment compared to baseline*

	0.25C & 0.25C		0.25 C & 0.3 C		0.25 C & 0.35C		0.25 C & 0.4C	
AOA	Cd increment	Percentage increment	Cd increment	Percentage increment	Cd increment	Percentage increment	Cd increment	Percentage Increment
0	0.00022	0.02%	0.00022	0.02%	0.00027	0.03%	0.00007	0.01%
2	0.00029	0.03%	0.00029	0.03%	0.00028	0.03%	0.00011	0.01%
4	0.00030	0.03%	0.00030	0.03%	0.00027	0.03%	0.00014	0.01%
6	0.00029	0.03%	0.00029	0.03%	-0.00012	-0.01%	0.00013	0.01%
8	0.00023	0.02%	0.00023	0.02%	0.00014	0.01%	-0.00008	-0.01%
10	0.00012	0.01%	0.00012	0.01%	-0.00001	0.00%	-0.00006	-0.01%

Based on the comprehensive analysis of both lift enhancement and drag reduction, the 0.25C & 0.40C groove configuration emerges as the most effective and aerodynamically advantageous design among all the tested configurations. This setup consistently demonstrates the highest percentage increase in lift coefficient (Cl), particularly at higher angles of attack such as 8° and 10°, where aerodynamic performance plays a crucial role in maintaining stability and preventing early flow separation. In addition to its lift advantage, this configuration also exhibits reduced or negligible increases in drag coefficient (Cd). It even shows drag reduction at certain AOAs compared to the baseline airfoil.

The superior performance of this configuration can be attributed to the strategic placement of the second groove further downstream at 0.40C along the chord, which likely helps re-energize the boundary layer. This configuration delays the flow over the surface for a longer duration, resulting in improved lift generation and reduced aerodynamic losses. This configuration achieves a more balanced aerodynamic profile compared to other groove placements, particularly those with closer spacing or more forward positioning, enhancing efficiency without introducing significant drag penalties. Therefore, the 0.25C & 0.40C configuration is strongly recommended as the optimal groove design, offering a favorable combination of improved lift and lower drag for applications where aerodynamic efficiency is critical.

3.6 Fixed Upper Groove (0.30C) and Variable Lower Configuration

This section investigates the aerodynamic performance of a dual-groove configuration, where the upper groove is fixed at 0.30C, and the lower groove is varied between 0.30C, 0.35C, and 0.40C along the lower surface. The goal is to evaluate how the second groove's location affects both lift and drag across a range of angles of attack (AOA) and to identify the most aerodynamically efficient design. By analyzing the lift coefficient (Cl) and drag coefficient (Cd), this comparison helps determine the most suitable lower groove position to pair with a fixed upper groove for enhanced overall performance.

3.6.1 Lift Coefficient Analysis of Fixed Upper Grove (0.30C)

This section analyzes how varying the lower groove position affects the airfoil's lift performance while keeping the upper groove fixed at 0.30C. The objective is to observe which configuration generates the highest and most consistent lift across different angles of attack.

Table 19 presents the lift coefficient data for the dual groove configuration with fixed upper grooves at 0.30C. The lift coefficient data shows that all three dual-groove configurations deliver lift values very close to the baseline, with slight variations depending on the lower groove position. At low angles (AOA = 0°–4°), the configuration with the lower groove at 0.35C shows a slightly higher Cl than the others, reaching 0.21550 at 2° and 0.42842 at 4°, which are marginally higher than the baseline and other designs. However, as AOA increases, the performance of this configuration becomes inconsistent. At 10°, it shows a lower Cl (1.03754) compared to both 0.30C & 0.30C (1.04090) and 0.30C & 0.40C (1.04020). The 0.30C & 0.40C configuration demonstrates the most stable and balanced lift behavior across all angles, closely matching or slightly exceeding the baseline at most points. This suggests that placing the second groove further aft on the lower surface (at 0.40C) may help delay flow separation and maintain good pressure recovery at higher AOAs. Fig. 20 shows a lift performance comparison across the same groove configurations. All designs closely follow the baseline curve, but 0.30C & 0.40C demonstrate a slight edge in lift at higher AOAs (especially at 8° and 10°), indicating improved suction and flow attachment. Meanwhile, 0.30C & 0.35C show less consistent behavior with a slight drop at 10°, making 0.30C & 0.40C the most balanced in terms of lift generation

Table 19 *Lift coefficient (Cl) for dual-groove configurations with fixed upper groove at 0.30C*

	Lift Coefficient			
AOA	**0.30C & 0.30C**	**0.30 C & 0.35 C**	**0.30 C & 0.40C**	**Baseline**
0	0.00015	0.00028	0.00062	0.00000
2	0.21410	0.21550	0.21480	0.21415
4	0.42720	0.42842	0.42791	0.42751
6	0.63779	0.63935	0.63818	0.63808
8	0.84323	0.84318	0.84379	0.84319

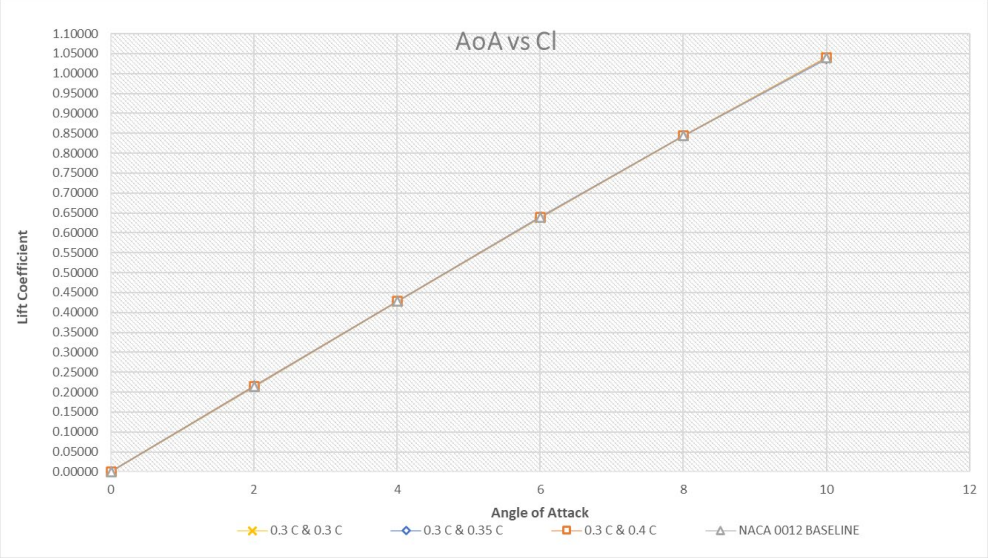

Fig. 20 *Lift coefficient (Cl) vs. angle of attack (AoA) for a fixed upper groove at 0.30C*

3.6.2 Drag Coefficient Analysis of Fixed Upper Grove (0.30C)

This section examines the drag characteristics for each dual-groove configuration. With the upper groove fixed at 0.30C, the comparison focuses on identifying which lower groove placement introduces the least aerodynamic resistance throughout the range of attack angles.

Table 20 presents the drag coefficient data for the dual groove configuration with fixed upper grooves at 0.30C. In terms of drag performance, all configurations show a slight increase in Cd compared to the baseline, with differences becoming more noticeable at higher AOA. At 0° to 4°, the 0.30C & 0.40C configuration consistently records the lowest drag among the groove setups, 0.00918 at 0° and 0.01040 at 4°, staying closest to the baseline

Progress in Aerospace and Aviation Technology Vol. 5 No. 1 (2025) p. 55-84

(0.00909 and 0.01021, respectively). As the angle increases to 10°, the drag penalty remains minimal for the 0.40C configuration (0.01706) compared to 0.30C & 0.30C (0.01689) and 0.30C & 0.35C (0.01719). Although the differences are small, this trend suggests that placing the second groove at 0.40C results in more favorable flow behavior with less aerodynamic resistance. Fig. 21 shows the variation of drag coefficient across different angles of attack for three dual-groove configurations with the upper groove fixed at 0.30C. All groove designs result in slightly higher drag than the baseline NACA 0012 airfoil. However, the 0.30C & 0.40C configuration consistently exhibits the lowest drag increase, indicating better aerodynamic efficiency. The difference becomes more noticeable at higher AOAs, where drag growth is more significant.

Table 20 *Drag coefficient (Cd) for dual-groove configurations with fixed upper groove at 0.30C*

	Drag Coefficient			
AOA	**0.30C & 0.30C**	**0.30 C & 0.35 C**	**0.30 C & 0.40C**	**Baseline**
0	0.00933	0.00926	0.00918	0.00909
2	0.00962	0.00956	0.00951	0.00937
4	0.01047	0.01041	0.01040	0.01021
6	0.01186	0.01187	0.01190	0.01167
8	0.01397	0.01413	0.01408	0.01384
10	0.01689	0.01719	0.01706	0.01685

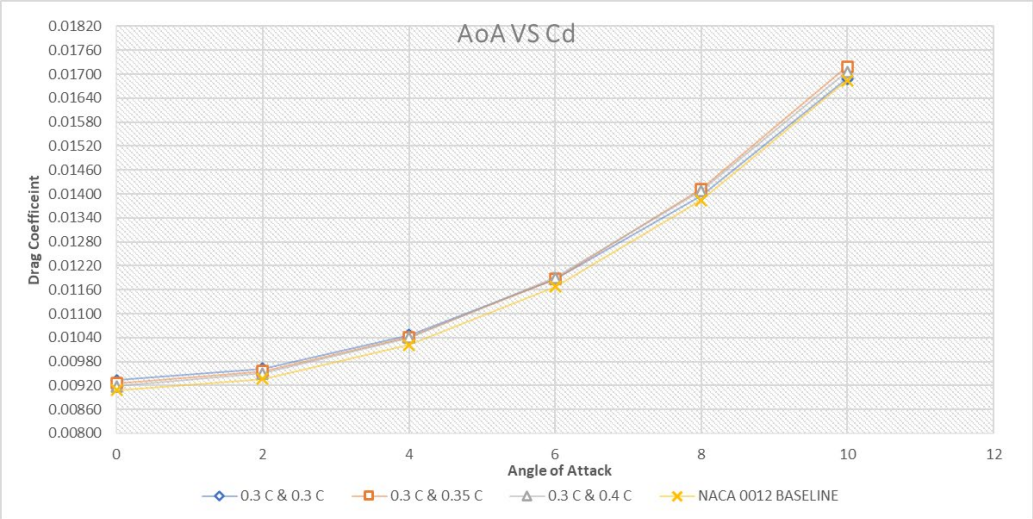

Fig. 21 *Drag coefficient (Cd) vs. angle of attack (AOA) for dual-groove configurations with fixed upper groove at 0.30C*

3.6.3 Comparison and Selection

This subsection evaluates the aerodynamic performance of dual-groove configurations where the upper surface groove is fixed at 0.30C, while the lower surface groove is varied at three different chordwise positions: 0.30C, 0.35C, and 0.40C. The analysis aims to explore how different placements of the lower groove affect flow behavior and the aerodynamic characteristics of the NACA 0012 airfoil. Specifically, the lift coefficient (Cl) and drag coefficient (Cd) differences and percentage changes are examined in comparison to the baseline airfoil with no grooves across a range of angles of attack (AOA). This evaluation helps determine which dual-groove configuration offers the best aerodynamic efficiency by achieving greater lift with minimal drag increase.

Table 21 shows the analysis of lift coefficient data for various groove configurations compared to the baseline. The analysis of lift coefficient data reveals that the 0.30C & 0.40C configuration provides a stable and consistent improvement in lift across most angles of attack. It shows positive lift gains at all AOAs, with the highest improvement of 0.08% at 10° AOA. The 0.30C & 0.35C configuration performs well at mid-range AOAs (2° to 6°), recording lift increases of up to 0.13%, but experiences a significant drop in lift at 10°, showing a negative difference of -0.18%. In contrast, the 0.30C & 0.30C configuration shows the highest Cl gain at 10° (0.15%) but underperforms at several other AOAs, including negative values at 2°, 4°, and 6°. These results suggest that while 0.30C & 0.30C may provide a localized benefit at high AOA, they lack consistency across the full AOA range.

Therefore, 0.30C & 0.40C are superior in terms of overall lift enhancement due to their balanced and positive performance.

Table 21 *Lift coefficient (Cl) difference and percentage change (compared to baseline)*

	0.30 C & 0.30 C		0.30 C & 0.35 C		0.30 C & 0.40 C	
AOA	Cl Increment	Percentage Increment	Cl Increment	Percentage Increment	Cl Increment	Percentage Increment
0	0.00015	0.02%	0.00028	0.03%	0.00062	0.06%
2	-0.00005	-0.01%	0.00135	0.13%	0.00065	0.06%
4	-0.00031	-0.03%	0.00090	0.09%	0.00040	0.04%
6	-0.00029	-0.03%	0.00127	0.13%	0.00010	0.01%
8	0.00004	0.00%	-0.00001	0.00%	0.00060	0.06%
10	0.00153	0.15%	-0.00183	-0.18%	0.00083	0.08%

Table 22 shows that the drag coefficient data at various groove configurations compared to baseline. All configurations show only slight increases in drag compared to the baseline, indicating that the addition of grooves does not significantly affect aerodynamic resistance. Among them, 0.30C & 0.40C consistently record the lowest drag increase, with Cd rising only by 0.01% to 0.02% across all AOAs. The 0.30C & 0.35C setup shows slightly higher drag, especially at 8° and 10°, reaching 0.03%, while 0.30C & 0.30C peaks at 0.03% but drops to 0.00% at 10°. Considering both lift and drag, 0.30C & 0.40C remain the most balanced and efficient configuration.

Table 22 *Drag coefficient (Cd) increment and percentage increment compared to baseline*

	0.30 C & 0.30 C		0.30 C & 0.35 C		0.30 C & 0.40 C	
AOA	Cd Increment	Percentage Increment	Cd Increment	Percentage Increment	Cd Increment	Percentage Increment
0	0.00025	0.02%	0.00017	0.02%	0.00009	0.01%
2	0.00025	0.03%	0.00019	0.02%	0.00014	0.01%
4	0.00025	0.03%	0.00020	0.02%	0.00019	0.02%
6	0.00019	0.02%	0.00020	0.02%	0.00023	0.02%
8	0.00013	0.01%	0.00029	0.03%	0.00024	0.02%
10	0.00004	0.00%	0.00034	0.03%	0.00021	0.02%

Considering both lift and drag performance, the 0.30C & 0.40C configuration is identified as the most optimal design when the first groove is fixed at 0.30C. It consistently improves lift across various angles of attack while maintaining minimal drag increase. Compared to other configurations, it shows stable aerodynamic behavior without significant performance drops. In contrast, 0.30C & 0.30C perform well only at high AOA but are inconsistent elsewhere, while 0.30C & 0.35C show lift gains at some angles but suffer from higher drag at others. Overall, 0.30C & 0.40C offer the best balance between lift enhancement and drag control, making them the most aerodynamically efficient choices.

3.7 Comparative Analysis of the Best-Performing Groove Configuration

This subsection presents a comparative evaluation of the three best-performing groove configurations identified from previous analyses. Table 23 shows the different configurations represent different groove placement strategies designed to improve the aerodynamic characteristics of the NACA 0012 airfoil. The analysis includes both lift (Cl) and drag (Cd) performance across a range of angles of attack. However, many airfoil applications prioritize lift enhancement as a key indicator of aerodynamic performance. The aim is to determine which configuration provides the best balance between maximizing lift and maintaining acceptable drag levels.

Progress in Aerospace and Aviation Technology Vol. 5 No. 1 (2025) p. 55-84

Table 23 *Summary of best-performing groove configurations*

Design type	Configuration name
Parallel	0.30C & 0.30C
Fixed Upper 0.25C Groove	0.25C & 0.40C
Fixed Upper 0.30C Groove	0.30C & 0.40C

3.7.1 Lift Coefficient (Cl) Comparison

Table 24 presents the lift performance of three selected groove configurations, 0.30C & 0.30C, 0.25C & 0.40C, and 0.30C & 0.40C, against the baseline NACA 0012 airfoil across varying angles of attack (AOA). Among these, the configuration with the fixed upper groove at 0.25C and lower groove at 0.40C consistently exhibits the most significant improvement in lift. It shows a positive percentage gain at all AOAs, reaching up to 0.66% at 8° and maintaining above 0.25% at the maximum AOA of 10°. This indicates a strong ability to energize the boundary layer and delay flow separation, especially at higher AOAs where aerodynamic performance is critical. The 0.30C & 0.40C configuration also shows positive lift gains across all angles, but with smaller improvements, typically under 0.1%. Meanwhile, the 0.30C & 0.30C design shows negative or negligible lift differences at low and moderate AOAs, only slightly improving at 10° with a 0.15% increase, making its lift performance less consistent. Considering the combined lift improvement across the AOA range, the 0.25C & 0.40C configuration is the most effective. It provides the highest and most consistent lift enhancement, making it the optimal design choice among the three configurations analyzed.

Table 24 *Lift coefficient (Cl) increment and percentage increment compared to baseline*

	0.30C & 0.30C		0.25C & 0.4C		0.3C & 0.4C	
AOA	Cl Increment	Percentage Increment	Cl Increment	Percentage Increment	Cl Increment	Percentage Increment
0	0.00000	0.00%	0.00069	0.07%	0.00062	0.06%
2	-0.00024	-0.02%	0.00082	0.08%	0.00065	0.06%
4	-0.00074	-0.07%	0.00086	0.09%	0.00040	0.04%
6	-0.00045	-0.05%	0.00102	0.10%	0.00010	0.01%
8	0.00004	0.00%	0.00658	0.66%	0.00060	0.06%
10	0.00147	0.15%	0.00263	0.26%	0.00083	0.08%

3.7.2 Drag Coefficient (Cd) Comparison

Table 25 presents the three groove configurations 0.30C & 0.30C, 0.25C & 0.40C, and 0.30C & 0.40C against the baseline NACA 0012 airfoil across varying angles of attack (AOA). The drag coefficient comparison reveals key differences in aerodynamic resistance across the three groove configurations. The 0.30C & 0.30C setup experiences significantly higher drag across all angles of attack, with an increase of up to 2.71% at AOA = 0° and still 0.24% at 10°, indicating a consistent and notable penalty in aerodynamic efficiency. In contrast, both 0.25C & 0.40C and 0.30C & 0.40C configurations show minimal increases in drag, typically between 0.01% and 0.02%, with some angles even experiencing a slight reduction, 0.01% at 8° and 10° for 0.25C & 0.40C. These two designs successfully maintain low aerodynamic resistance while still improving lift. Between the two, 0.25C & 0.40C display the most favorable drag characteristics, showing either negligible or negative changes compared to the baseline, indicating enhanced efficiency without compromise. Thus, when considering drag performance alone, 0.25C & 0.40C again emerge as the best design due to their ability to reduce or minimally impact drag while enhancing lift.

Table 25 *Drag coefficient (Cd) increment and percentage increment compared to baseline*

	0.30C & 0.30C		0.25 C & 0.4C		0.3C & 0.4C	
AOA	Cd increment	Percentage increment	Cd increment	Percentage increment	Cd increment	Percentage increment
0	0.02708	2.71%	0.00007	0.01%	0.00009	0.01%
2	0.02672	2.67%	0.00011	0.01%	0.00014	0.01%
4	0.02475	2.48%	0.00014	0.01%	0.00019	0.02%
6	0.01602	1.60%	0.00013	0.01%	0.00023	0.02%
8	0.00925	0.92%	-0.00008	-0.01%	0.00024	0.02%
10	0.00241	0.24%	-0.00006	-0.01%	0.00021	0.02%

3.7.3 Lift and Drag Change Comparison at 10° Angle of Attack

To highlight the aerodynamic performance of the best groove configurations, this subsection presents a comparative bar chart analysis focusing on lift gain and drag change at a high angle of attack (AOA = 10°). This AOA was selected because it represents a critical condition where flow separation is more likely and differences in aerodynamic behavior become more apparent. The comparison helps to identify which configuration provides the most efficient lift enhancement while minimizing drag penalties. Fig. 22 compares the increase in lift coefficient (Cl) for the three selected groove configurations relative to the baseline NACA 0012 at an angle of attack of 10°. The configuration with the upper groove fixed at 0.25C and the lower groove at 0.40C °C shows the highest lift gain. Fig. 23 displays the increase or decrease in drag coefficient (Cd) for the same configurations. The parallel 0.30C & 0.30C design shows the highest drag penalty, while the 0.25C & 0.40C configuration records the lowest drag change, with a slight reduction from the baseline.

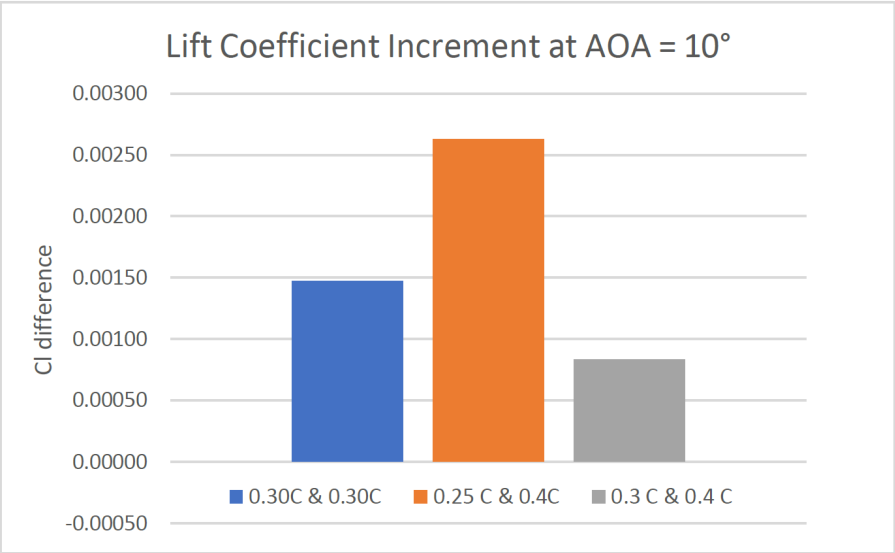

Fig. 22 *Lift Coefficient increment at AOA = 10°*

Progress in Aerospace and Aviation Technology Vol. 5 No. 1 (2025) p. 55-84

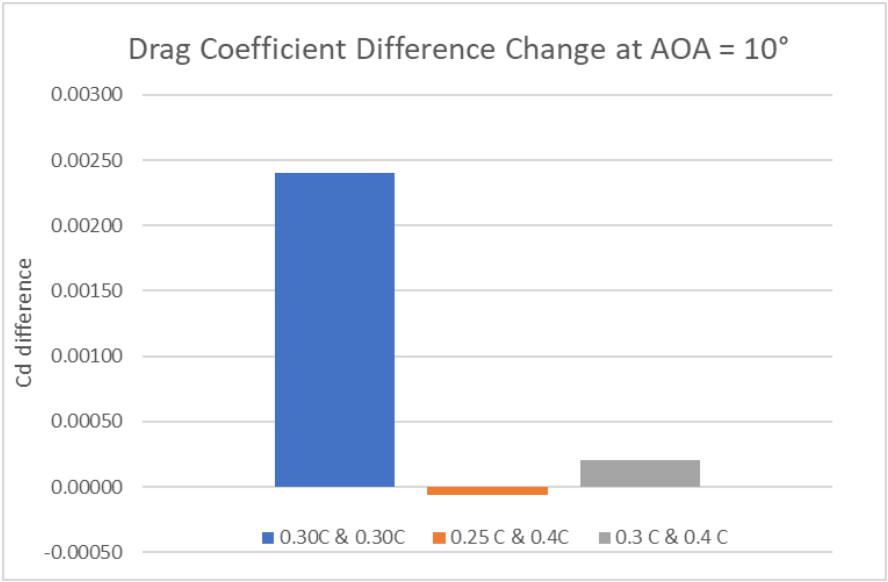

Fig. 23 *Drag coefficient difference change at AOA = 10°*

Based on the comparative analysis of lift and drag performance across the three best-performing groove configurations—parallel groove at 0.30C & 0.30C, fixed upper groove at 0.25C with lower at 0.40C, and fixed upper groove at 0.30C with lower at 0.40C—the configuration with the upper groove at 0.25C and lower groove at 0.40C emerges as the most aerodynamically efficient design. This configuration consistently demonstrates the highest lift coefficient increase, particularly at higher angles of attack, while maintaining minimal or even negative drag penalties compared to the baseline airfoil. The pressure coefficient analysis and performance metrics reinforce its effectiveness in energizing the boundary layer and enhancing flow attachment. Therefore, the 0.25C & 0.40C groove arrangement is recommended as the optimal groove configuration, offering a well-balanced solution for improving aerodynamic efficiency without compromising drag characteristics, making it suitable for practical applications in performance-critical aerodynamic surfaces.

3.7.4 Pressure Coefficient (Cp) Distribution of Selected Groove Design

Fig. 24 shows the pressure coefficient (Cp) distribution comparing the baseline airfoil with a modified design featuring a fixed groove at 0.25C on the upper surface and 0.40C on the lower surface. The baseline curve follows a typical pressure profile for the NACA 0015 airfoil, with a strong suction peak near the leading edge and smooth pressure recovery toward the trailing edge. In the modified design, slight deviations in Cp are observed near the groove locations. The groove at 0.25C (upper surface) affects the suction region, while the groove at 0.40C (lower surface) introduces small changes in the pressure region. These local disturbances suggest the grooves alter boundary layer behavior without significantly changing the overall Cp trend.

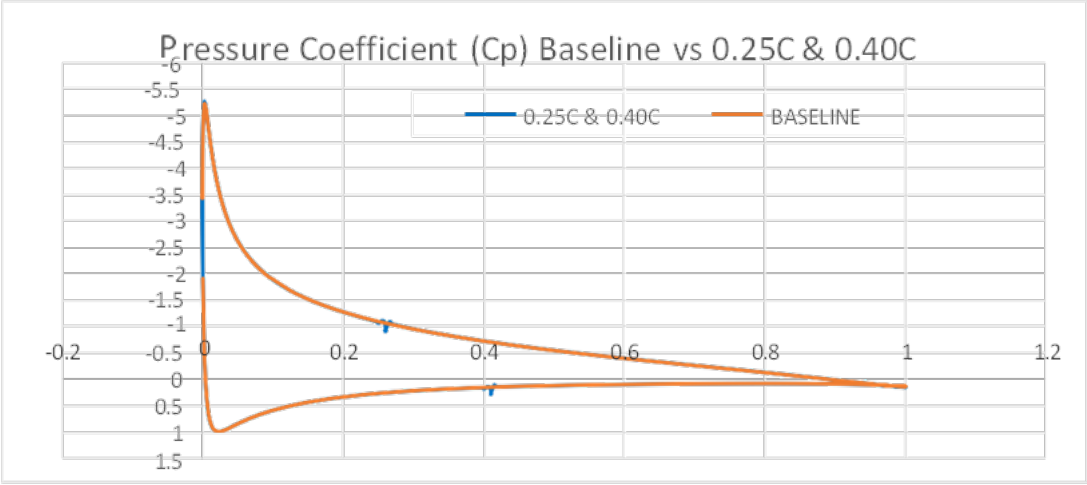

Fig. 24 *Pressure coefficient (Cp) baseline vs. 0.25C & 0.40C at 10°*

3.7.5 Velocity Contour

This section presents the velocity and pressure contours for the airfoil with a fixed groove at 0.25C (upper surface) and 0.40C (lower surface), compared to the baseline airfoil across angles of attack (AoA) from 0° to 10°. Table 26 shows the velocity contour for NACA0012 (baseline) and 0.25C & 0.40C groove configurations, while Table 27 shows the velocity contour at the groove at the upper and lower surfaces of the airfoil. The velocity contour shows higher flow acceleration on the upper surface, especially at higher AoA. Disturbances near the 0.25C groove indicate local boundary layer interaction that may help delay separation. Compared to the baseline, the modified design maintains more attached flow at higher AoA. On the lower surface, the 0.40C groove causes minimal disruption.

Table 26 *Velocity contour for baseline and 0.25C & 0.40C*

AoA	Baseline	0.25C & 0.40C
0°	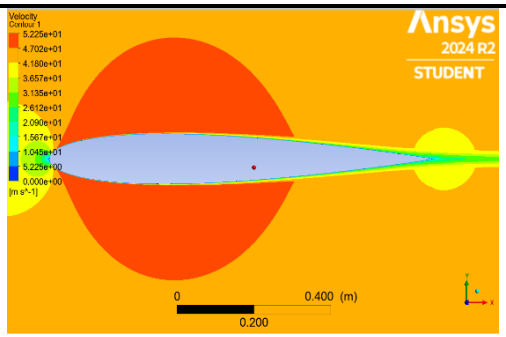	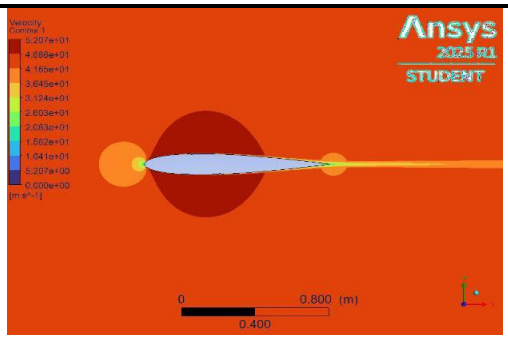
2°	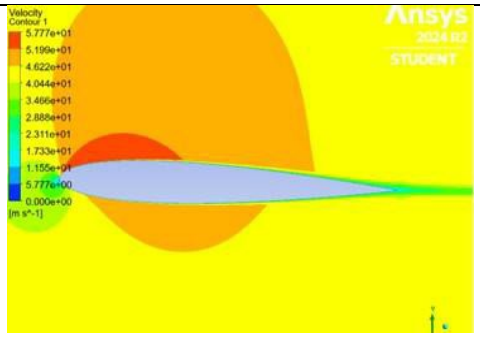	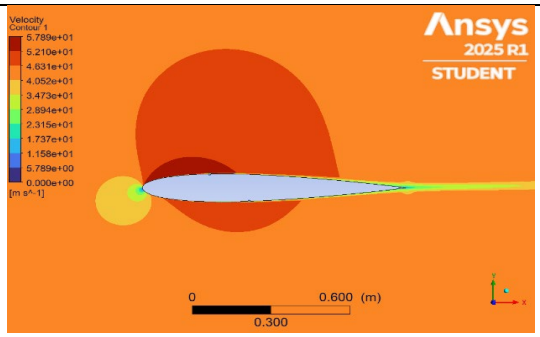
4°	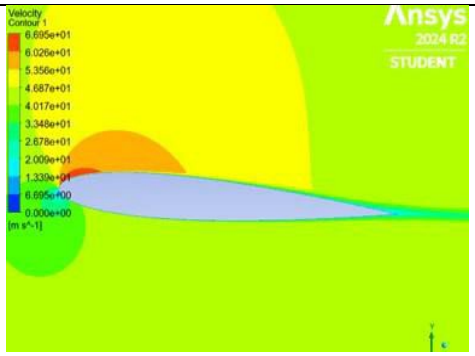	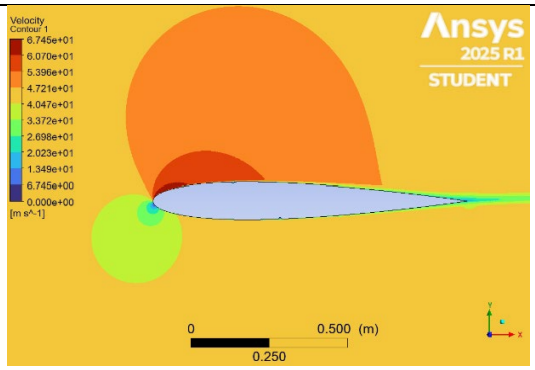
6°	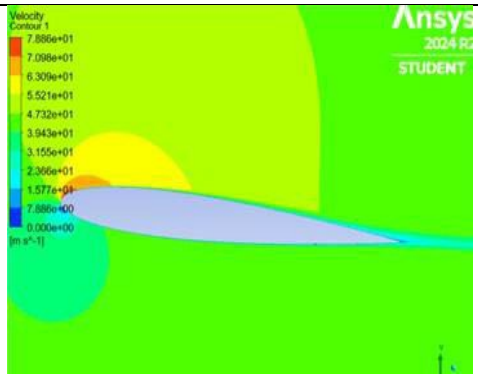	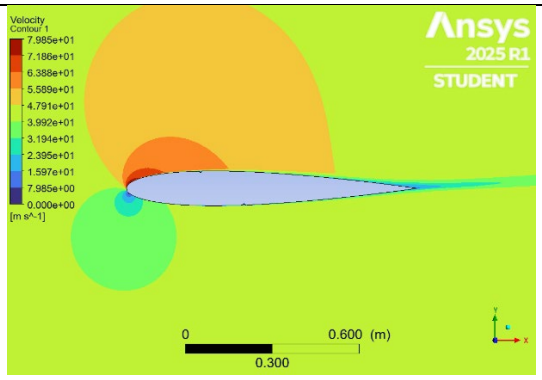

Progress in Aerospace and Aviation Technology Vol. 5 No. 1 (2025) p. 55-84

8°	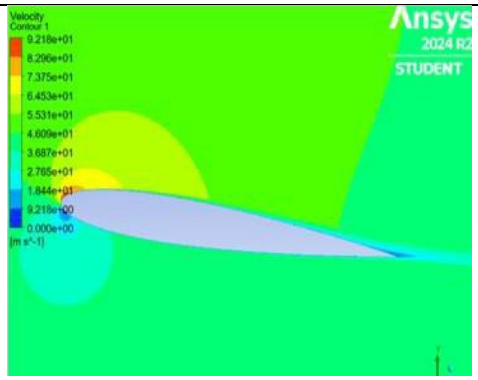	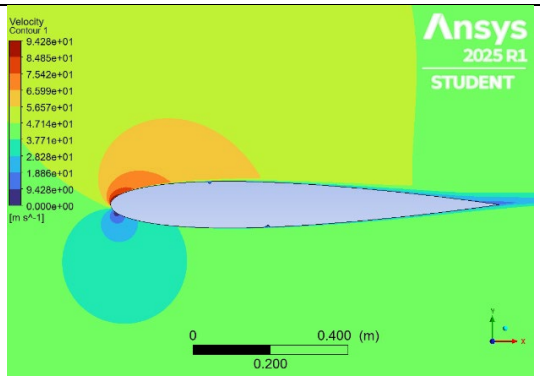
10°	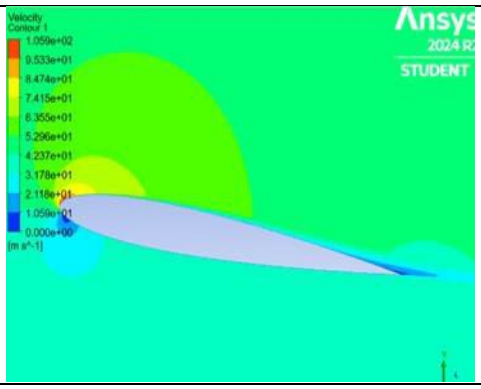	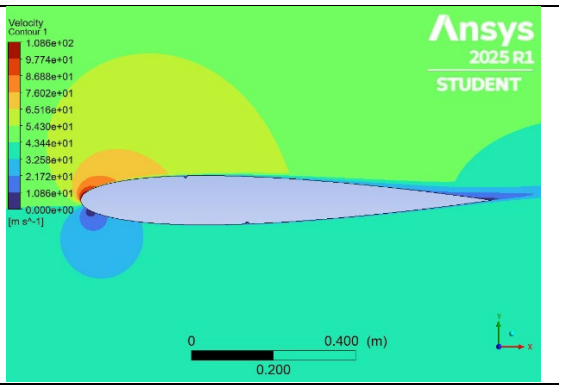

Table 27 *Velocity contour at groove*

0.25C upper surface & 0.40C lower surface

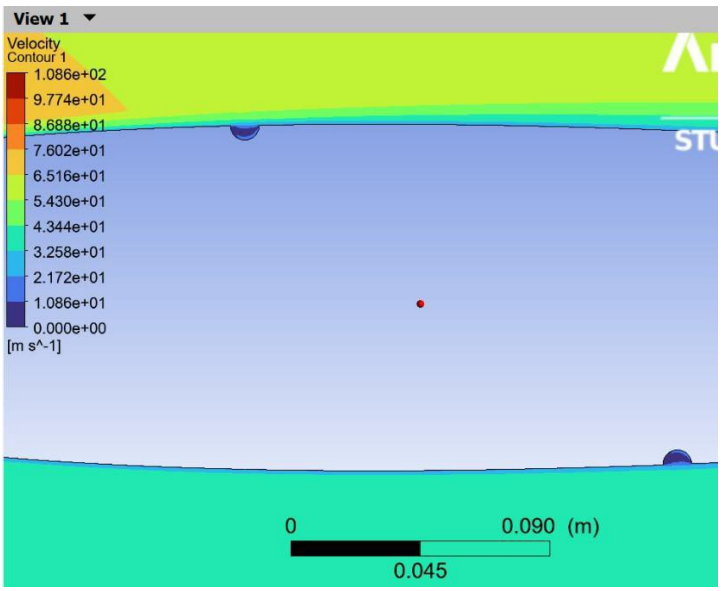

Groove at Upper Surface

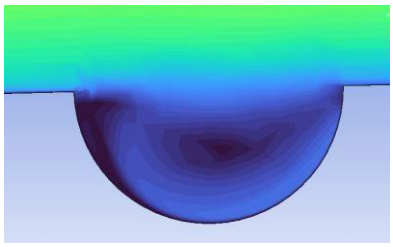

Groove at Lower Surface

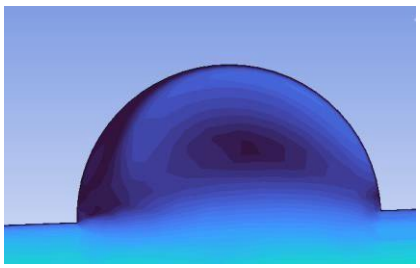

4. Conclusion

This study investigated the aerodynamic performance of a NACA 0012 airfoil modified with a single groove on both the upper and lower surfaces under low angles of attack ranging from 0° to 10°. The simulations were conducted using ANSYS Fluent to evaluate various groove configurations in terms of size and placement, with a focus on lift, drag, and pressure distribution. The implementation of passive flow control through geometric surface modifications aimed to enhance airfoil performance in low-speed conditions. The simulation results revealed that the use of grooves significantly influenced the aerodynamic behavior of the airfoil. Among the tested groove diameters, 1.0 cm showed the most balanced aerodynamic performance, while excessively large or small grooves offered less improvement. Placement of the grooves also played a critical role, with the most effective configuration observed when the upper groove was fixed at 0.25C and the lower groove at 0.40C. This combination

resulted in the highest lift coefficient and a slight reduction in drag compared to the baseline airfoil. Validation against established experimental data confirmed that the simulation setup was accurate, with acceptable deviation in lift coefficient values. Mesh independence testing further ensured that the numerical results were reliable and not dependent on grid density. Through comparative analysis, it was also shown that grooved airfoils performed better than the baseline at higher low angles of attack (especially 8°–10°), indicating that surface grooves help delay flow separation and improve flow attachment. The dual-groove design provided better performance than single-surface configurations due to the symmetrical influence on both suction and pressure sides of the airfoil. This study has demonstrated the potential of using simple, passive surface modifications to enhance airfoil performance under low-speed conditions, contributing to future airfoil design strategies for UAVs and similar applications.

Acknowledgement

This research was conducted with the support of the Faculty of Mechanical and Manufacturing Laboratories at Universiti Tun Hussein Onn Malaysia (UTHM). The computational resources provided by UTHM were instrumental in conducting simulations for this study.

Conflict of Interest

Authors declare that there is no conflict of interest regarding the publication of the paper.

Author Contribution

The authors confirm their contribution to the paper as follows: ***study conception and design:*** *Muhammad Aideed Azman, Mohd Fauzi Yaakub;* ***data collection:*** *Muhammad Aideed Azman;* ***analysis and interpretation of results:*** *Muhammad Aideed Azman, Mohd Fauzi Yaakub, Esmail Abdullah, Wan Muhammad Aqil Wan Nawang;* ***draft manuscript preparation:*** *Muhammad Aideed Azman. All authors reviewed the results and approved the final version of the manuscript.*

References

[1] Kundu, P. K., Cohen, I. M., Dowling, D. R., & Capecelatro, J. (2024). Aerodynamics. In Fluid Mechanics (7th ed., pp. 151–174). Elsevier.

[2] Suprayitno, Yu, J. C., Aminuddin, & Wulandari, R. (2020). Airfoil aerodynamics optimization under uncertain operating conditions. Journal of Physics: Conference Series, 1440(1), Article 012014. https://doi.org/10.1088/1742-6596/1440/1/012014.

[3] Ismail, A. K., Kasim, M. U., Balogun, M. B., Abdullah, M. B., Faru, F. T., & Ibrahim, I. U. (2020). Effect of angle of attack on lift, drag, pitching moment, and pressure distribution of NACA 4415 wing. Journal of Science Technology and Education, 8(1), 1–10.

[4] Kilavuz, A., Ozgoren, M., Durhasan, T., Sahin, B., Kavurmacioglu, L., Akilli, H., & Sarigiguzel, F. (2021). Analysis of attack angle effect on flow characteristics around torpedo-like geometry placed near the free surface via CFD. Politeknik Dergisi, 24(4), 1579–1592. https://doi.org/10.2339/politeknik.675632.

[5] Klose, B. F., Spedding, G. R., & Jacobs, G. B. (2021). Direct numerical simulation of cambered airfoil aerodynamics at Re=20,000. arXiv. https://doi.org/10.48550/arXiv.2108.04910.

[6] ElJack, E. M., & Soria, J. (2018). Bursting and reformation cycle of the laminar separation bubble over a NACA-0012 aerofoil: Characterisation of the flow-field. arXiv. https://doi.org/10.48550/arXiv.1807.04573.

[7] Akbar, M. A., Hariyadi, S., & Mahaputra, R. P. (2020). Effect of angle of attack on airfoil NACA 0012 performance. R.E.M. (Rekayasa Energi Manufaktur) Journal, 5(1), 35–40. https://doi.org/10.21070/rem.v5i1.1235.

[8] Ashby, D. L., & Fowlkes, A. P. (2016). Aerodynamic characteristics of the NACA 0012 airfoil in the presence of external flow distortions (NASA Langley Research Center Technical Report). NASA.

[9] Abbott, I. H., von Doenhoff, A. E. (1959). Theory of wing sections. Dover Publications, Inc., New York.